Summer 7-31-2024

CASTOR OIL-BASED POLYURETHANE ADHESIVES: EFFECT OF CROSS-LINKER ON THE BOND STRENGTH

Mayankkumar Chaudhary
Pittsburg State University, mayankkumarlakshmanbhai.chaudhary@gus.pittstate.edu

CASTOR OIL-BASED POLYURETHANE ADHESIVES: EFFECT OF CROSS-LINKER ON THE BOND STRENGTH

A Thesis Submitted to the Graduate School
in Partial Fulfilment of the Requirements
For the Degree of
Master of Science

Mayankkumar L. Chaudhary

Pittsburg State University

Pittsburg, Kansas

July 2024

CASTOR OIL-BASED POLYURETHANE ADHESIVES: EFFECT OF CROSS-LINKER ON THE BOND STRENGTH

Mayankkumar L. Chaudhary

APPROVED:

Thesis Advisor _____
Dr. Ram K. Gupta, Department of Chemistry

Committee Member _____
Dr. Khamis Siam, Department of Chemistry

Committee Member _____
Dr. Timothy Dawsey, National Institute for Materials and advancement

Acknowledgment

I am immensely thankful to Dr. Ram K. Gupta, my supervisor extraordinaire, whose wisdom, unwavering support, and boundless creativity have been the wind beneath my academic wings. Dr. Gupta's guidance has been akin to navigating through a labyrinth with a seasoned guide, always leading me toward illuminating insights and innovative pathways. His commitment to excellence and penchant for pushing boundaries have transformed my research journey into a thrilling adventure. With heartfelt appreciation, I thank Dr. Gupta for his invaluable time, tireless dedication, and unwavering belief in my potential, which have been the catalysts for my academic growth and success. I also want to thank the faculty members, especially Dr. Khamis Siam and Dr. Tim Dawsey, for their constructive remarks and academic contributions, which significantly improved the quality of my thesis. Their faith in my ability has been the driving force behind my achievements. Special gratitude goes to my friends Dr. Rutu, Palak, Kiran, Pratik, Sonu, and Sujal for providing academic and moral support and fostering a positive and inspiring atmosphere where I could grow and develop. I deeply thank my father, Mr. Lakshmanbhai B. Patel, and my mother, Mrs. Madhuben L. Bhatol, whose unconditional love and unwavering support have been the cornerstone of my journey. They have been my greatest source of inspiration, providing selfless love and guidance at every turn. Throughout my educational pursuit, my parents have stood by me, offering both emotional and financial support, for which I am profoundly grateful. I would also like to thank the Department of Chemistry and the National Institute for Materials Advancement at Pittsburg State University for their financial support, which made this study possible. This thesis would not have been feasible without the collaborative efforts of these individuals and organizations. Thank you for being an important part of my educational endeavour.

CASTOR OIL-BASED POLYURETHANE ADHESIVES: EFFECT OF CROSS-LINKER ON THE BOND STRENGTH

An Abstract of the Thesis by
Mayankkumar L. Chaudhary

Adhesives are important for binding diverse materials, promoting structural integrity and functional versatility in countless daily life applications. An enormous obstacle remains in the development of polyurethane (PU) adhesives exhibiting excellent bonding strength. Designing a chain extender with appropriate molecular structures is critical to improving the bonding strength of PU-based adhesives. In this work, PU-based adhesive was prepared using castor-oil-based polyol (COP) and diisocyanate. The bonding strength of the adhesive was improved by adding chain extenders such as N, N-bis(2-hydroxyethyl) thiophene-2,5-dicarboxamide (ETP) and N, N-Bis(2-hydroxyethyl)-terephthalamide (ETAM). The modified adhesive showed high bonding strength after the addition of chain extenders due to the presence of the dicarboxamide group, which served as a center for hydrogen bonding. The bonding strength of PU adhesive increased to 7.22 and 9.68 MPa from 5.0 MPa after the addition of 7.5 wt.% of ETP and 5.0 wt.% of ETAM, respectively. The bonding strength of the adhesives was tested on both wood (oak) and metal (stainless steel) coupons. The bonding strength of 9.68 MPa on oak wood and 6.73 MPa on stainless steel coupon was observed for the 5.0 wt.% of ETAM-based PU adhesive. The bonding failure was observed to be due to wood failure. The reason behind the good bonding is noncovalent bonds which are formed between the functional group of the PU molecular chain and the surface of the substrate. In addition, no major changes in Fourier transform infrared (FT-IR) spectroscopy after keeping these adhesives in different solvents were observed. Good

crosslinking is also confirmed by studying the gelling and swelling data of the adhesives.

TABLE OF CONTENTS

LIST OF TABLES

LIST OF FIGURES

LIST OF SCHEMATICS

LIST OF ABBREVIATIONS

CO	Castor-oil
COP	Castor-oil polyol
DMF	Dimethyl formamide
DMSO	Dimethyl sulfoxide
DSC	Different scanning calorimetry
DTD	Dimethyl thiophene-2,5-dicarboxylate
DTG	Derivative thermogram
DTP	Dimethyl terephthalate
EA	Ethanol amine
ETAM	N, N-Bis(2-hydroxyethyl)-terephthalamide
ETP	N, N-bis(2-hydroxyethyl) thiophene-2,5-dicarboxamide
FT-IR	Fourier transform infrared spectroscopy
GPC	Gel permeation chromatography
MDI	Methylene diphenyl diisocyanate
NIPU	Non-isocyanate polyurethane
NMR	Nuclear Magnetic Resonance
NMP	N-methyl-2-pyrrolidone
PU	Polyurethanes
TEAB	Tetraethylammonium bromide
TGA	Thermogravimetric analysis
THF	Tetrahydrofuran
UV	Ultraviolet
VO	Vegetable oil
WCA	Water contact angle

CHAPTER I

INTRODUCTION

PU is an extremely versatile class of polymers utilized in various applications such as insulators, foams, elastomers, synthetic skins, coatings, and adhesives. It was originally developed by Dr. Otto Bayer and his colleagues through fundamental diisocyanate polyaddition reactions [1]. In 1937, PU reached industrial-scale synthesis and became established in the market by the 1950s. PU are characterized by the presence of a urethane linkage and can be easily synthesized through an addition reaction between alcohol and isocyanate. However, to prepare PU, both starting materials must have a functionality of at least 2. **Figure 1** provides the reaction and the general formula of PU. PU are extensively explored due to their simple synthesis, which can be carried out at room temperature and under mild conditions. Structural modifications in polyols or isocyanates can be easily achieved using various chemical methods, offering PU a range of properties. For instance, an elastic PU can be synthesized using a polyol with a linear structure, high molecular weight, and low functionality. Conversely, a rigid PU can be produced by using a polyol with aromatic groups, low molecular weight, and higher functionality for cross-linking [2]. A balance between hydrophobic and hydrophilic elements in the chemical structure yields water-dispersible PU suitable for coating applications.

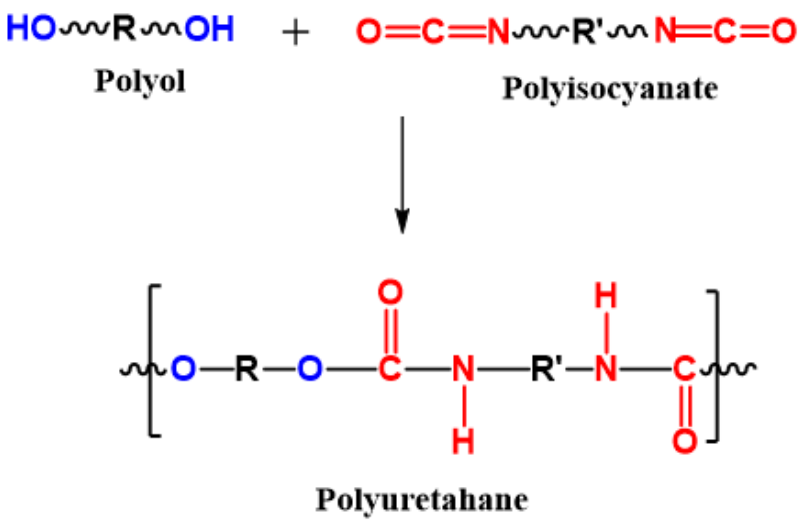

Figure 1. General reaction scheme for the synthesis of PU through polyaddition reaction between diols and isocyanates

PU is one of the most significant classes of industrial polymers, boasting the fastest-growing global market. This growth is attributed to the ability to modify the starting materials to produce a variety of PUs with specific properties. The global market for PU was valued at over $65 billion and is projected to grow at a rate of 3.2% until 2027. Utilizing PU foams as thermal insulators in housing can reduce energy consumption by 75% to 95%, leading to both economic and sustainable benefits [3]. To be specific, the PU market is usually segmented into five uneven parts including foams, coatings, elastomers, adhesives, and the biomedical field, as displayed in **Figure 2** [4][5]. PU's high electrical resistance makes them ideal for electrical insulation and dielectric applications in electronic devices. Their lightweight nature, combined with high mechanical strength, renders them essential in the automotive industry for improving efficiency through reduced fuel consumption, enhanced safety, and greater comfort. Flexible foams are extensively used in the automotive and furniture sectors, appearing in beds, couches, and seat cushions. Additionally, flexible PU are utilized in the footwear industry as shock absorbers in shoes and in the packaging industry to

safeguard shipments from damage. Their chemical inertness and environmental stability also make PU well-suited for use in adhesives and anticorrosion coatings.

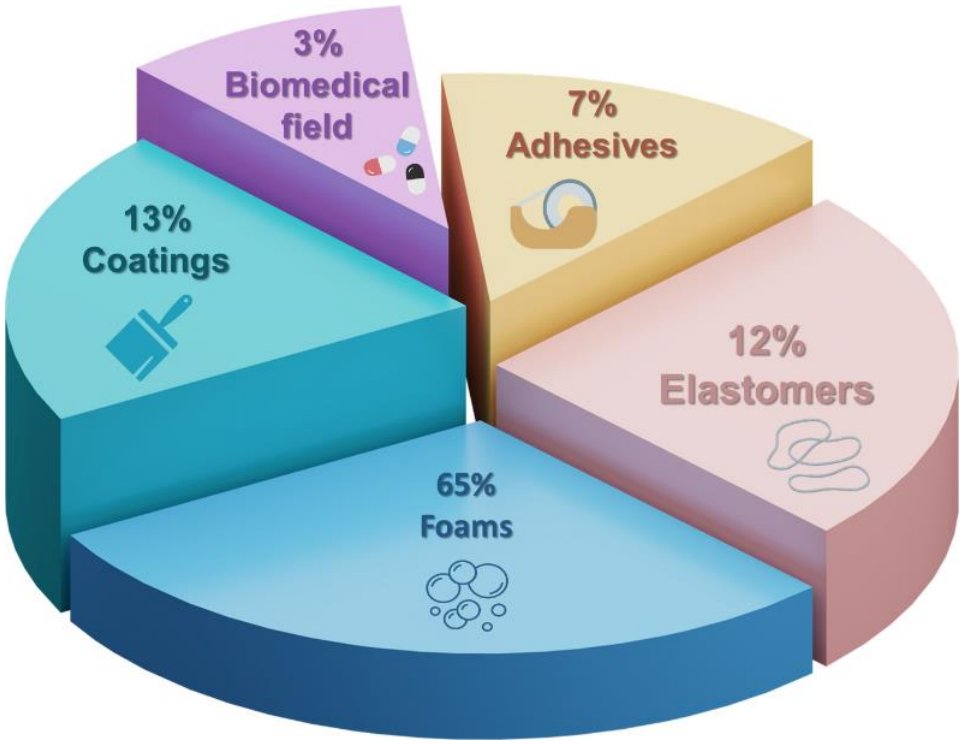

Figure 2. PU market share in 2022 by application

Corrosion, which leads to an average gross domestic product loss of 3% in many countries, has made anticorrosion coatings a significant area of interest. PU's novel applications in biomedical and tissue engineering are facilitated by their chemical stability, high surface area, and flexibility. These applications include synthetic scaffolds for cell culture and materials that assist in fluid transport within the body, such as synthetic veins or pacemaker components [6]. The tuneable properties of PU make them uniquely suitable for a variety of applications, as previously mentioned. However, despite their widespread use and significant market presence, certain issues like the high flammability of PU foams limit their application and warrant scientific attention. Furthermore, most chemicals used in PU production are derived from petroleum-based resources, raising sustainability and toxicity concerns. The instability and degradation of PU in outdoor applications also require attention. Efforts are being made to use

renewable resources to synthesize the starting chemicals for PU, promoting a sustainable future [7] . In the realm of adhesive technology, there is a renewed interest in traditional bio-based binders like starch and renewable rubber. Additionally, more recent technologies are being applied, such as using modified vegetable oils (VOs) or lignin derivatives for binder synthesis.

Today, a broad range of adhesive technologies can utilize renewable materials, which may offer equal or superior performance compared to their petroleum-based counterparts. However, the mere use of renewable materials in a product is often insufficient for commercialization, particularly if additional costs are involved in materials or their implementation, especially when they are not direct replacements for existing technology. Nonetheless, plant-based materials can introduce properties previously unattainable, such as new structural elements, high monomer functionalities, and the high molecular weight of starting materials. These characteristics promote the formation of densely cross-linked networks and enhance adhesion to various substrates. Notable bio-based building blocks include VOs, which can increase adhesive hydrophobicity and water resistance, as well as biopolymers like proteins, polysaccharides, and lignin, and bio-based monomers such as isosorbide and itaconic acid, all of which can enhance adhesive performance in various ways.

1.1 Overview of different adhesive types

The term "adhesive" encompasses a broad spectrum of materials and applications (**Figure 3**). Although the primary function is always to bond separate substances, this bonding is accomplished through various mechanisms and according to diverse specifications [8]. In an adhesive joint, there is typically a polymeric substance that forms connections with the substrate through chemical bonds, physiochemical

attractions, and physical interlinking. The way this polymer is applied is just as crucial as its chemical makeup because it dictates the conditions required for application and thus the potential end uses. Additionally, it affects aspects like the spread of the adhesive on the substrate and the contact area, both of which significantly influence the adhesive forces that can be generated [9].

While there are still some adhesives that are applied in solution, this practice is becoming less common. In this method, the solvent evaporates, leaving behind the final joint. However, due to environmental considerations, dispersions, where the polymer is suspended in water, are gaining popularity as an alternative. Both solvent-based adhesives and dispersion adhesives can be formulated using materials such as polyvinyl acetates, PU, acrylates, and natural and synthetic rubber [10].

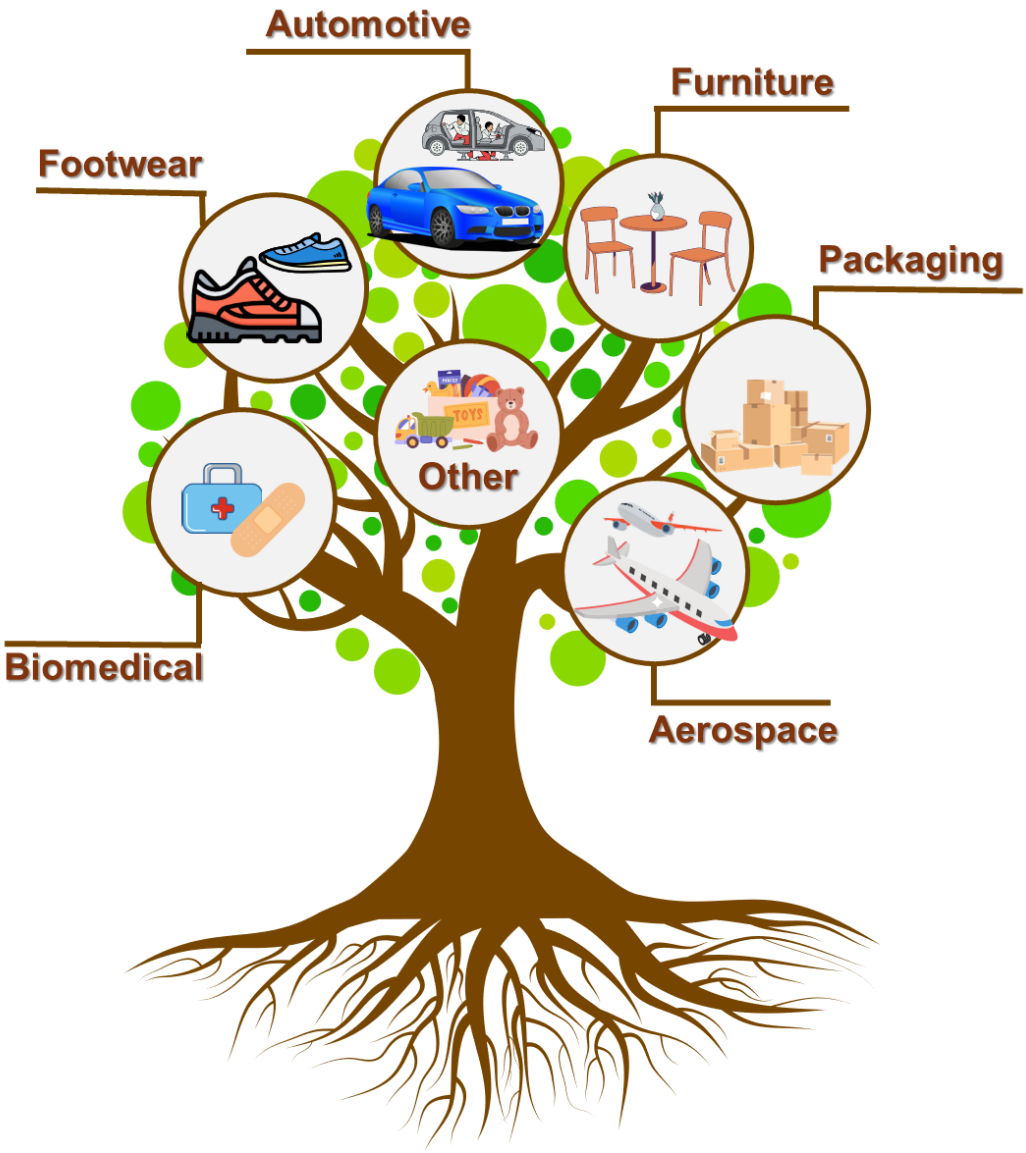

Figure 3. Application of adhesive in different sectors

Another application method is employed for hot-melt adhesives. The primary benefit of hot-melt adhesives is their rapid bonding time, making them preferred for processes with high throughput requirements. These adhesives involve melting the polymer and applying it while hot, with the joint hardening as the adhesive cools. Typically, hot-melt adhesives are formulated using thermoplastic polymers like polyamides, saturated polyesters, and ethylene-vinyl acetate copolymers [10]. Lastly, there are adhesives applied prior to the complete formation of the polymer. The joint solidifies through a chemical reaction of the components, making these adhesives reactive. They are

classified into 1-component reactive adhesives, where all reactive components are contained in a single component, and two-component reactive adhesives, where the reactive substances are mixed shortly before application [10].

In 1-component reactive adhesives, the adhesive joint formation usually begins with an external trigger. For example, water initiates the reaction in PU, silane, and cyanoacrylate adhesives, while anaerobic adhesives require the absence of air, and condensation resins like phenol formaldehyde, urea formaldehyde, or melamine formaldehyde adhesives need high temperatures to start the process. These condensation resins are commonly utilized in the wood construction sector to bond wood and wood composite materials [11]. Another instance involves acrylates, which are cured using ultraviolet light (UV). This UV light activates a photo-initiator compound, initiating a radical polymerization reaction. two-component reactive adhesives may be formulated with epoxides, PU or methacrylates. While epoxides and PU undergo addition reactions, methacrylates, such as acrylates, undergo radical polymerization, which begins upon mixing with an initiator compound [10]. The various adhesive categories are not always entirely separate, as hybrids like reactive hot-melt adhesives exist. These adhesives consist of a blend of polymers, where one polymer rapidly cools while the other continues to undergo chemical reactions, merging the quick application of hot-melt adhesives with the enhanced cohesion and longevity of reactive adhesives [12].

A final, somewhat distinct category of adhesives comprises pressure-sensitive adhesives. These adhesives stand out because they do not harden but maintain their tackiness over their service life, relying predominantly on non-covalent interactions with the substrate. Pressure-sensitive adhesives are frequently formulated using

acrylates, rubbers, and UV-curing polymers, and find applications, such as in adhesive tapes and labels [12].

1.2 Motivations for the use of sustainable adhesives

In recent times, there has been a growing emphasis across the chemical industry to enhance the sustainability of both processes and products. This shift is driven partly by increased environmental consciousness among consumers and resulting regulations, as well as concerns about the impending scarcity of oil, a primary source of many chemicals, and the potential volatility in petroleum prices. Within the adhesive sector, this trend is most evident in the transition from solvent-based to water-based or high solid adhesives, alongside a renewed focus on traditional natural adhesive materials like polysaccharides and proteins [13]. Another motivation for developing adhesives derived from renewable sources is the shift towards a circular economy. Utilizing bio-renewable or waste feedstock aids in diminishing the carbon footprint. Additionally, renewable materials such as starch, polyhydroxyalkanoates, or cellulose often possess greater inherent biodegradability compared to synthetic materials like polypropylene and polyethylene [13]. Although most adhesives are currently derived from petroleum, the recent classification of formaldehyde as a hazardous substance provides further motivation to explore alternative adhesive options, particularly in the wood industry. Many wood adhesives, used for both solid wood and wood composites, still contain formaldehyde-based condensation resins. To mitigate harmful emissions during production and throughout the product's lifespan, alternative adhesives are needed. This has spurred increased research into eco-friendlier and renewable alternatives, such as protein-based adhesives.

Apart from regulatory pressures, another factor influencing investment in the adhesive market is the need for new, sustainable products. As highlighted in a 2015 report by Frost & Sullivan titled "Investment Analysis of the European Adhesives and Sealants Market," the adhesive market is fiercely competitive, driving the development of customized, specialized products to differentiate and enhance customer loyalty. In the construction sector, as analyzed in the report "North American and European Construction Adhesives and Sealants Market, forecast to 2022," there is a growing demand for high-performance products, particularly ones offering superior shock, heat, moisture, and UV resistance. Conversely, the non-structural adhesives market is increasingly focused on user-friendly technologies that offer formulation flexibility. In the automotive sector, the emphasis is on lightweight vehicles to reduce carbon emissions. Hence, there's a need for adhesive solutions that bond lightweight materials and facilitate recycling while minimizing hazardous substances. Some of these challenges can be addressed using the unique properties of renewable materials. Consequently, these market trends present an excellent opportunity to explore the introduction of sustainable adhesives into portfolios to benefit both the environment and profitability. Here in this research, VO was used to synthesize bio-based PU adhesive. VOs are a better replacement of petroleum-based polyol as they contain triglycerides and unsaturation in their structure which can be modified by several methods to make VO based polyol for PU production. Castor oil (CO) was used in this research as bio-based polyol.

1.3 Chemistry of castor oil

CO is distinguished as the top choice among VOs because of its structural preferences, natural biodegradability, affordability, low toxicity, industrial feasibility, and

widespread availability [14][15]. Because of its extensive use in coatings, adhesives, foams, sealants, and encapsulation materials, significant research has been conducted using CO as a polyol source in lieu of petroleum-based products [16]. **Table 1** displays the composition of CO, including its acid content and average percentage range. The table indicates that ricinoleic acid is predominant in CO, with an approximate double bond value of 3.04 and three hydroxyl groups (-OH) associated with its structure. With an average functionality of 2.7, CO is deemed a suitable candidate for use as a crosslinking monomer in the synthesis of PU prepolymer. A variety of PU materials, ranging from flexible foams to elastomers to rigid foams, have been developed using CO as a natural polyol with attached hydroxyl groups. [17]. Primarily, the structural characteristics of CO make it well-suited for direct use as a polyol in the formation of PU films with desirable properties. For instance, the long-chain fatty acid composition enhances properties such as water repellency, toughness, and resistance to acids [18]. A broad spectrum of properties, ranging from soft elastomers to hard plastics with tailored physical and mechanical characteristics, have been achieved by adjusting the structural composition through variations in the amount of CO, chain extender, or reaction conditions [14]. The uniform distribution of hydroxyl groups within CO triglycerides promotes the formation of a consistent crosslinked network in the resulting PUs.

Table 1. The fatty acid composition and physio-chemical characteristics of CO

Fatty acid	Molecular formula	Properties	
Palmitic	$C_{16}H_{32}O_2$	Appearance:	Light yellow
stearic	$C_{18}H_{36}O_2$	Specific gravity at 40℃:	0.946
Oleic	$C_{18}H_{34}O_2$	Acid value (mg KOH /g):	1.27-3
Linolenic	$C_{18}H_{32}O_2$	Hydroxy value (mg KOH /g):	156-165
Linolenic	$C_{18}H_{30}O_2$	Saponification value (mg KOH /g):	180

Ricinoleic	$C_{18}H_{34}O3$	Viscosity (ninherent 0.2% THF at 25℃)	0.06

1.4 Objective of this research

Formaldehyde and melamine-based wood adhesives are popular for their good bonding strength and durability, but they are hazardous to climate and human health. Traditional methods for the synthesis of polyol are based on fossil fuels, these components are non-renewable and will be depleted soon. Hence, this research aims to find an alternative to petroleum-based wood adhesive without using solvents or catalysts. In this study, CO is used as raw material to synthesize polyol for PU adhesive. CO was converted into an isocyanate-reactive polyol through epoxidation and ring-opening reaction. The modification of polyol was confirmed by FT-IR spectroscopy, hydroxyl value evaluation, and gel permeation chromatography (GPC). This research aimed to analyze the effect of crosslinkers such as ETP, ETAM on the properties of PU adhesive. The bonding strength of adhesives was tested on oak wood, and stainless-steel substrate. This research examined the physical properties, mechanical characteristics, and thermal stability of the adhesive made from COP.

CHAPTER II

MATERIALS AND METHODS

2.1 Materials

CO was purchased from Walmart (Pittsburg, KS, USA). 2,5-thiophenedicarboxylic acid (2,5-TDCA), sulfuric acid (H_2SO_4), dimethyl terephthalate (DTP), ethanol amine (EA), methylene diphenyl diisocyanate (MDI), glacial acetic acid (99.7%), hydrogen peroxide (H_2O_2) (29%), toluene (99.5%), Amberlite IR 120H, sodium chloride, sodium sulfate, tetrafluoro boric acid (HBF_4) (48 wt.%), Lewitt MP 64 (99.8%), and methanol (99.9%) were purchased from Fisher Scientific (Allentown, PA, USA).

2.2 Synthesis of dimethyl thiophene-2,5-dicarboxylate

2 g of 2,5-TDCA were added with 20 ml of concentrated sulfuric acid (H_2SO_4) in a round-bottom flask and heated to 80 °C for 3 hours. After the reaction mixture was cooled to room temperature, 20 ml of methanol (CH_3OH) was added slowly, and then refluxed for 24 hours. After cooling to ambient temperature, the reaction mixture was filtered to separate the product. The synthesized product was washed with distilled water and then dried in a vacuum oven at 80 °C for 4 hours to get white crystals of dimethyl thiophene-2,5-dicarboxylate (DTD) (**Scheme 1**).

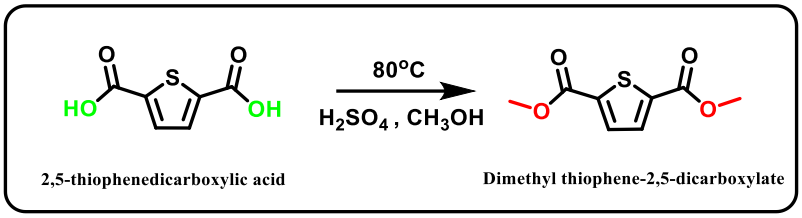

Scheme 1. Synthesis of DTD from 2,5-TDCA

2.3 Synthesis of N, N-bis(2-Hydroxyethyl) thiophene-2,5-dicarboxamide

1 g of DTD was dissolved in 15 ml methanol at 50 °C, followed by the addition of 0.76 g of EA. The mixture was stirred at 50 °C for 24 h to ensure that the reaction was fully completed. The solvent was then removed by a rotary evaporator. Through the difference in solubility of the product and raw material in acetone, the mixture was washed with acetone several times and filtered to obtain ETP as a white solid (**Scheme 2**).

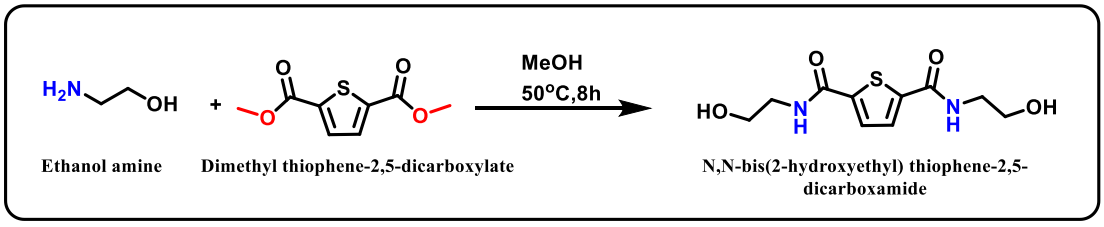

Scheme 2. Synthesis of ETP from DTD

2.4 Synthesis of N, N-bis(2-Hydroxyethyl)-Terephthalamide

3.8 g of DTP was dissolved in 50 ml methanol at 50 °C, followed by the addition of 3.6 g of EA. The mixed solution was stirred at 50 °C for 24 h to ensure that the reaction was fully completed. The solvent was then removed by a rotary evaporator. Through the difference in solubility of the product and raw material in acetone, the mixture was washed with acetone several times and filtered to obtain ETAM as a white solid (**Scheme 3**).

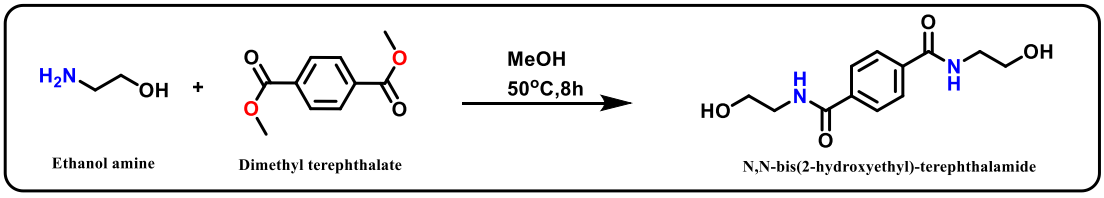

Scheme 3. Synthesis of ETAM from DTP

2.5 Synthesis of castor oil-based polyol

2.5.1. Epoxidation of castor oil

In the three-necked round bottom flask, 500 g of CO having a hydroxyl value of 122 mg KOH/g and an iodine value of 82 gI_2/100g, 250 g of toluene and 125 g of Amberlite resin were added. After that, 49 ml of glacial acetic acid was gradually added dropwise for 30 minutes using a dropping funnel, while ensuring that the temperature remained in the range of 5-8 °C. The reaction was then stirred for 30 minutes. Subsequently, a total of 272 ml of hydrogen peroxide with a concentration of 30% was added gradually, while maintaining the temperature between 5-10 °C. After adding H_2O_2 completely, the temperature was raised to 70 °C, and the system was left to run for 7 hours while being continuously monitored. Upon completion of the reaction, the mixture exhibited a color transition from orange to yellowish. Subsequently, the reaction mixture was filtered. Concurrently, a 10 wt.% brine solution was prepared. Afterward, the reaction mixture was washed 7 times with brine solution to remove inorganic impurities. After completing it, anhydrous sodium sulfate (Na_2SO_4) was added to remove moisture. The mixture was filtered, and the resulting liquid was then dried using rotary evaporation for 3 hours. The resulting product was analyzed using FT-IR and GPC (**Figure 1**). Later, the epoxidized castor oil (ECO) was used for the preparation of polyol using the process given below.

2.5.2. Ring opening of epoxidized castor oil

COP was synthesized as follows. The relative mass of methanol was calculated according to the 7:1 molar ratio of ECO and methanol. Tetrafluoroboric acid (HBF_4) at a concentration of 0.05% of the total weight of the reaction mixture was chosen as a catalyst. The desired amounts of methanol and HBF_4 were added to a three-necked round-bottomed flask, and the temperature slowly increased to 65-70 ℃ with continuous stirring. ECO was then added dropwise over 50 minutes. The reaction mixture was refluxed for 90 minutes after the complete addition of ECO. After the reaction solution was cooled to room temperature, the required amount of Lewatit MP 64 resin was added and stirred for another 45 minutes to catalyze the ring-opening reaction by removing extra protons from the system. The molar ratio of Lewatit MP 64 to HBF4 was adjusted to be 3:1. After the reaction mixture was separated from the resin, rotary evaporation was performed for 3 hours to remove trace amounts of moisture and unreacted methanol. The reaction scheme for the synthesis of ECO and COP is shown in **Scheme 4**. Some of the important characteristics of CO, ECO, and COP are given in **Table 2**. Structural characterizations of CO, ECO, and COP using FT-IR and GPC are shown in **Figure 1**.

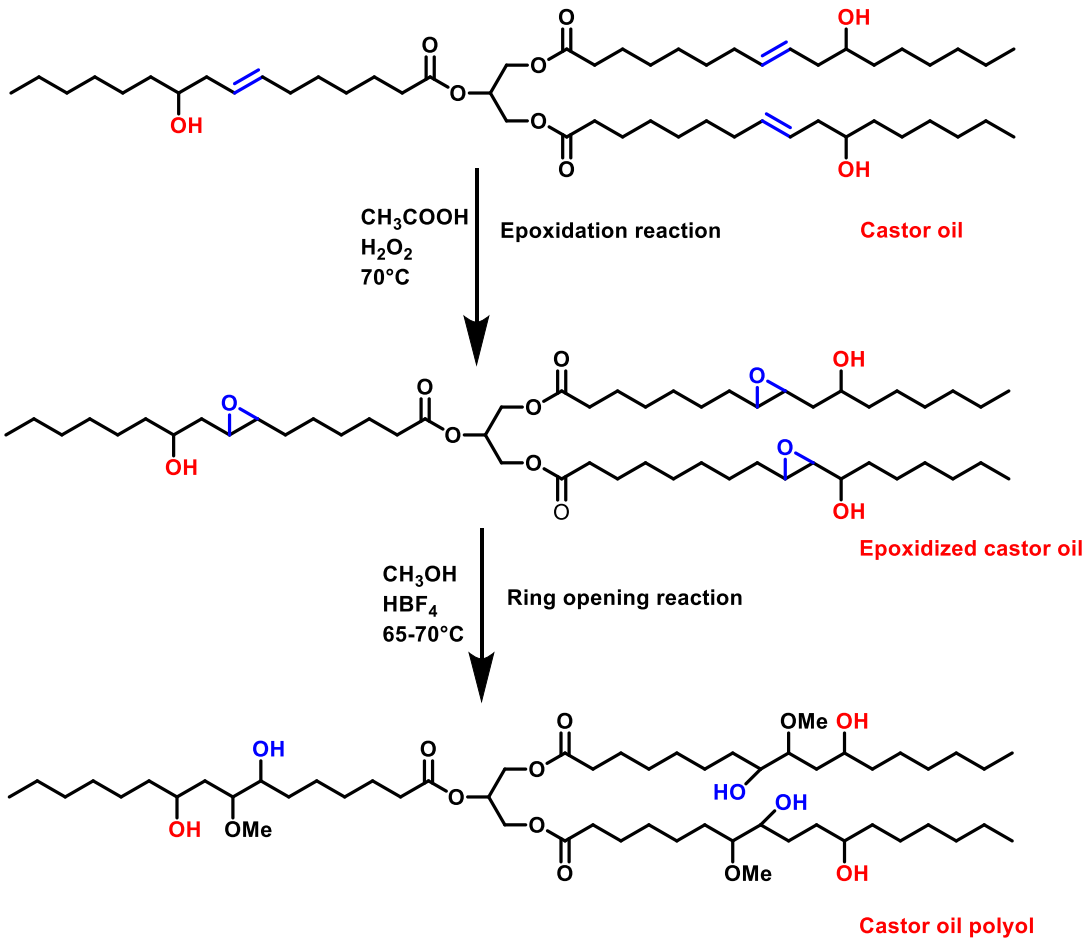

Scheme 4. Reaction scheme for the synthesis of COP

Table 2. Some of the characteristics of CO, ECO, and COP

Tests	Units	CO	ECO	COP
Iodine value	$gI_2/100g$	82.79	0.2	-
Epoxy-oxirane oxygen value	%	-	4.88	2.70
Hydroxyl value	mg KOH/g	122	-	270
Acid value	mg KOH/g	3.67	-	0.73
Viscosity @ 25°C	Pa.s	0.41	2.06	8.83

2.6 Preparation of adhesive

Adhesive samples were prepared at room temperature by adding polyol and diisocyanate with varying amounts of chain extenders (**Scheme 5**). The details of the

amount of polyol, diisocyanate, and chain extenders are provided in **Table 3** and **Table 4**. To study the bonding strength, oak wood, and stainless-steel specimens were chosen. The adhesives were applied to an area of a dimension of 27.5 mm by 27.5 mm (length x width). All the samples were prepared in the same way and three specimens were made for each sample to get the average bonding strength of the adhesive.

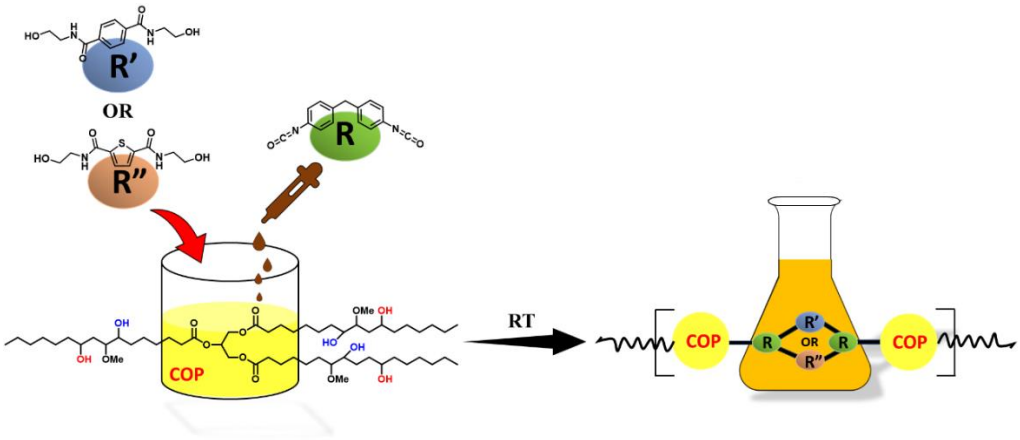

Scheme 5. Schematic diagram of PU adhesives

Table 3. Details of ETP-based PU adhesive samples

Sample code	COP (g)	MDI (g)	ETP (g)	Wt.%
ETP -0	1	0.65	0	0
ETP -2.5	1	0.68	0.025	2.5
ETP -5.0	1	0.71	0.050	5
ETP -7.5	1	0.74	0.075	7.5
ETP -10.0	1	0.77	0.100	10

Table 4. Details of ETAM-based PU adhesive samples

Sample code	COP (g)	MDI (g)	ETAM (g)	Wt.%
ETAM -0	1	0.65	0	0
ETAM -2.5	1	0.67	0.025	2.5
ETAM -5.0	1	0.70	0.050	5
ETAM -7.5	1	0.72	0.075	7.5
ETAM-10.0	1	0.75	0.100	10

2.7 Characterization methods and technique

2.7.1 Iodine value

The iodine value is used to determine the degree of unsaturation present in a fat or oil. Unsaturated fatty acids contain double bonds, and the iodine value indicates how many grams of iodine can be reacted by 100 g of fat or oil [19]. Here, the number of double bonds in soybean oil was confirmed by the Hanus titration method.

2.7.2. Epoxide number

The epoxide number indicates the number of epoxide groups (oxirane rings) per unit mass or unit of a certain functional group in a molecule. Glacial acetic acid and tetraethylammonium bromide (TEAB) were used. To perform this test, 0.2 g of epoxidized soybean oil was dissolved in 50 mL of TEAB solution. For titration, 0.1 N perchloric acid was taken and titration was performed after adding a drop of crystal violet as an indicator to the solution. The titration was completed when the color changed from blue to green, and the measured volume helped to determine the amount of epoxy present in the epoxidized soybean oil. This test was repeated 2 more times and

the average value of a total of 3 tests was taken for confirmation then further reaction of soybean polyol was performed.

2.7.3. Hydroxyl value

The hydroxyl number is a measure of the amount of hydroxyl (OH) group in a chemical compound. It is an important parameter to confirm the -OH value of polyol, which provides information about the functionality and the required number of isocyanates for an effective chemical reaction. In this work, ASTM-D 4274, (the phthalic anhydride pyridine (PAP)) technique was used. First, in a glass bottle, 10 mL of hydroxyl solution was mixed with 0.6 g of soybean polyol. The bottles were loosely capped and placed in a preheated oven at 100°C for 70 minutes. During that time, the solution was shaken every 15 minutes. The mixture was then settled down at room temperature, and 10 mL of HPLC-grade water and 20 mL of isopropanol were added. This mixture was mixed for 10 min. Lastly, the titration was done by the addition of 1 N NaOH until a pink colour appeared. The amount was calculated and the hydroxyl number.

2.7.4. Acid value

The acid value, as determined using the IUPAC 2.202 standard procedure, around 1 g of the sample was dissolved in 30 mL of the solvent mixture (isopropanol, toluene, and phenolphthalein indicator). Then after 0.1 N potassium hydroxide was added gradually until a pink colour shift was observed. The measurements were used to calculate the acid value. For the castor oil polyol formulation 0.37 mg KOH/g which means that 0.37 mg of potassium hydroxide (KOH) was required to neutralize the acidic components present in one gram of castor oil polyol.

2.7.5 Fourier-transform infrared spectroscopy

FT-IR is a quick and efficient method for detecting particular functional groups inside a chemical molecule. This technique is used for obtaining the infrared spectrum of a solid, liquid, or gas's absorption or emission. Unlike other tests, it removes the requirement for sample purification and does not use solvents. The materials' FTIR spectra were recorded using a PerkinElmer Spectrum Two Spectrophotometer (**Figure 4**). The scans spanned the spectrum range of 4000-400 cm^{-1} with a resolution of 4 cm^{-1} and an average of 64 scans, allowing for a quick and thorough study of the chemical composition. FTIR spectroscopy has been utilized in various areas, including chemistry, materials science, pharmaceuticals, food analysis, and environmental monitoring.

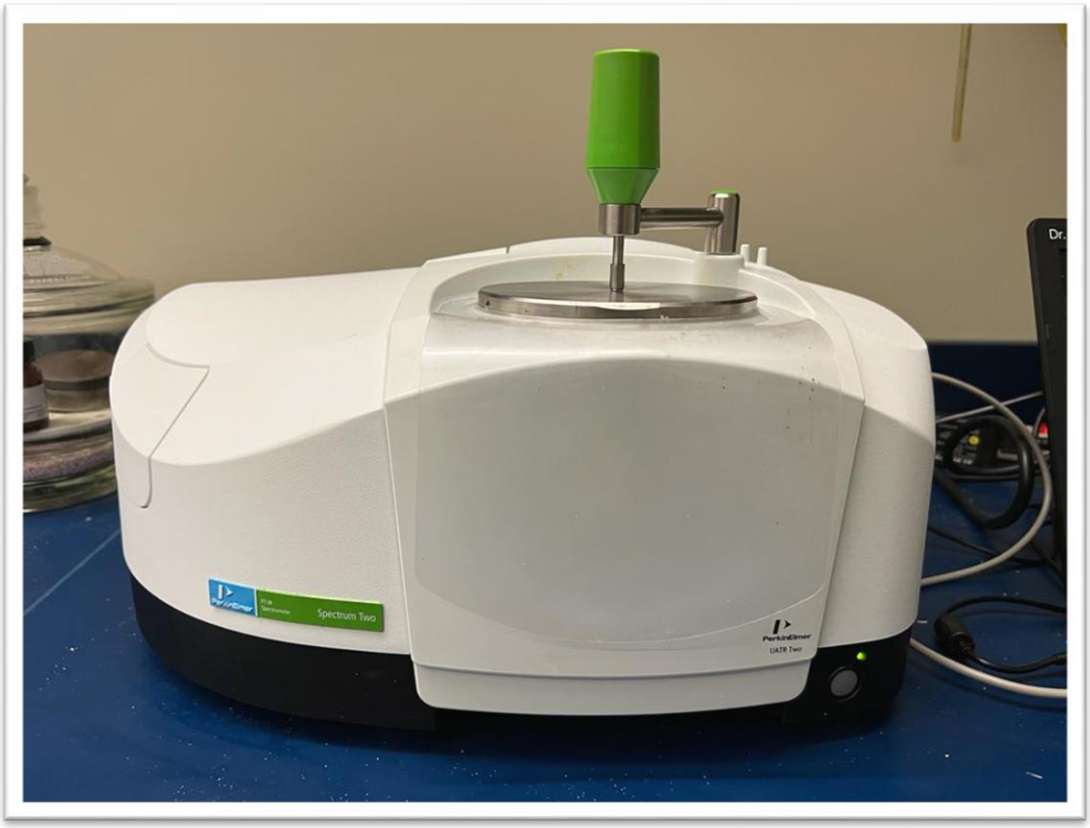

Figure 4. Digital photo of FT-IR instrument used in this research

2.7.6 Viscosity

Viscosity is the measurement of the resistance of the flow of a substance. Viscosity is directly proportional to molecular weight. If molecular weight is high viscosity should be high. An AR 2000 dynamic stress rheometer (TA instruments, USA) as shown in **Figure 5** was used for this testing. The viscosity was measured at 25°C with shear stress increasing from 1 to 2000 Pa linearly. The dynamic rheometer was equipped with a cone plate having an angle of 2° and a cone diameter of 25 mm.

Figure 5. AI 2000 dynamic stress rheometer for measuring viscosity

2.7.7. Gel permeation chromatography

GPC, also known as Size Exclusion Chromatography (SEC), stands as a pivotal technique in polymer science, enabling the separation and analysis of macromolecules based on their size in solution. Particularly instrumental in polymer characterization, GPC's ability to differentiate polymers according to molecular size provides crucial insights into the distribution of molecular weights within a polymer sample. This information is essential for assessing polymer quality, understanding synthesis processes, and predicting material properties. In the polymer sector, GPC plays a key role in quality control, ensuring the consistency of polymer batches and aiding in the characterization of complex hydrocarbons. In this study, the GPC instrument from Waters, located in Milford, MA, USA, was employed, as illustrated in **Figure 6.** Additionally, tetrahydrofuran (THF) served as the solvent, flowing at a rate of 1 mL/min and maintained at a temperature of 30 °C.

Figure 6. The GPC instrument used in this research

2.7.8. Nuclear magnetic resonance

Nuclear magnetic resonance (NMR) spectroscopy is a sophisticated analytical technique that provides detailed insights into the structure, composition, and dynamics of molecules. At its core, NMR relies on the behaviour of atomic nuclei when subjected to a strong magnetic field and radiofrequency radiation. When placed in a magnetic field, certain nuclei, such as hydrogen or carbon, align themselves in two energy states. By applying radiofrequency radiation at the resonant frequency corresponding to the energy difference between these states, the nuclei can be excited, and their response is detected by the NMR spectrometer. The resulting NMR spectrum provides a wealth of information about the molecule being analyzed. The positions of peaks in the spectrum correspond to the resonant frequencies of different nuclei within the molecule, while

the intensities of the peaks reflect the abundance of those nuclei. Additionally, the shapes and splitting patterns of peaks reveal details about the local chemical environment and interactions between neighbouring nuclei. This allows researchers to determine the molecular structure, identify functional groups, elucidate molecular dynamics, and even monitor chemical reactions in real time. NMR spectroscopy finds widespread applications across various fields, including chemistry, biochemistry, pharmaceuticals, materials science, and more. In chemistry, NMR is used for structural elucidation of organic and inorganic compounds, determining stereochemistry, and studying reaction mechanisms. In biochemistry, it plays a crucial role in studying protein structure, dynamics, and interactions, as well as in metabolomics and drug discovery. Moreover, NMR is utilized in quality control, forensic analysis, environmental monitoring, and geological studies, showcasing its versatility and importance in modern scientific research and analysis. The Magritek spinsolve 80 MHz NMR Spectrophotometer as shown in **Figure 7** was utilized to obtain spectral data for synthesized materials.

Figure 7. Digital photo of NMR instrument used in this research

2.7.9. Thermogravimetric analysis

Thermogravimetric analysis (TGA) is a technique for determining the thermal stability of materials by heating them at an even rate and measuring the weight change of the sample with temperature. To assess the thermal stability of NIPU films with varying diamine and different curing times, samples were subjected to analysis using the TGA instrument (Q500, Discovery, Trios, USA), as illustrated in **Figure 8.** A sample of approximately 5-10 mg was placed on an aluminium pan and the test was conducted under nitrogen flow at a ramp rate of 10°C/min within a temperature range of 25–600°C.

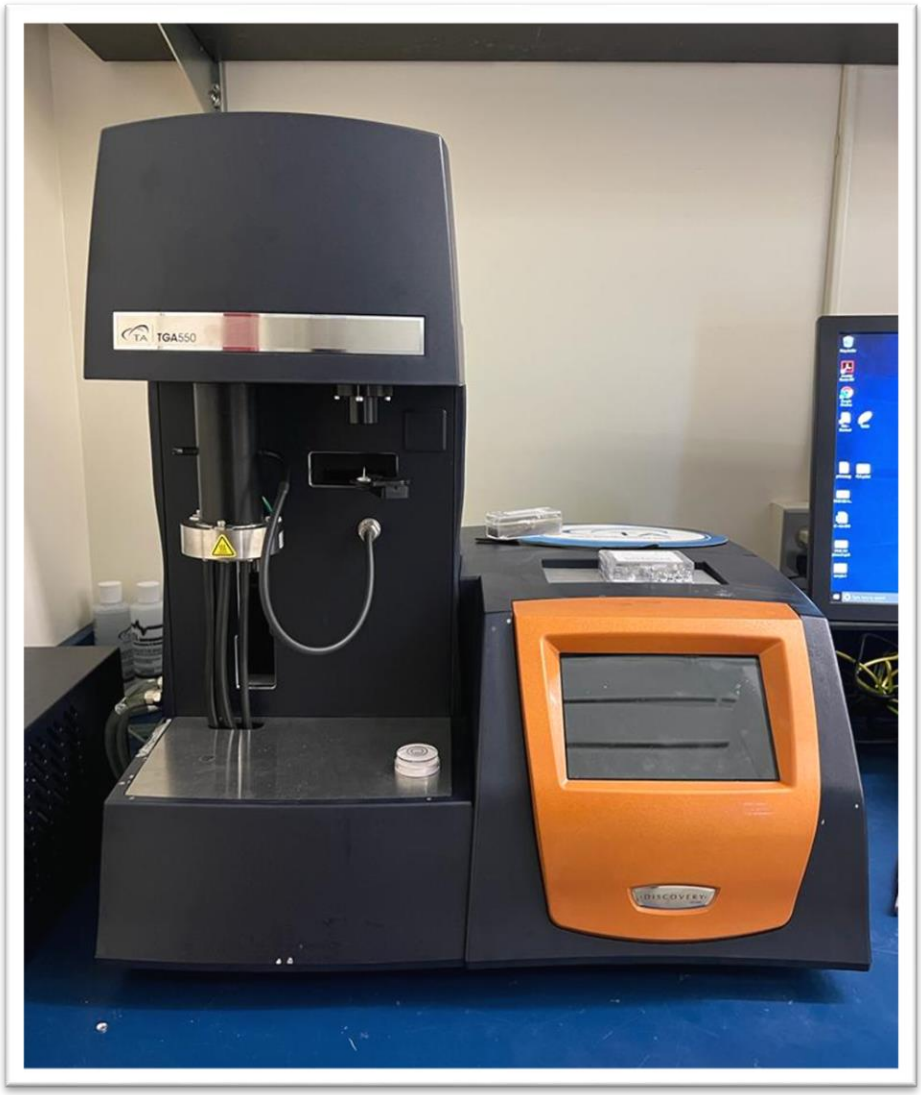

Figure 8. Digital photo of the TGA analysis instrument used in this research

2.7.10 Differential scanning calorimetry

Different scanning calorimetry (DSC) is an instrument used for thermal analysis to evaluate changes in the physical characteristics of samples and their temperature over time. This instrument is primarily used to measure glass transition temperatures (Tg), melting temperatures (Tm), and crystallization temperatures (Tc). All the DSC tests for this study were carried out using the DSC Q100 instrument (TA Instruments, USA) as shown in **Figure 9.** All the tests were performed in the temperature range of -80 to 300° C with a ramp rate of 10° C per minute. DSC gives understanding by measuring thermal stability, identifying phases, and separating between amorphous and crystalline regions. It is useful to understand how chemicals are distributed in different crystal structures. DSC also measures the melting point and heat absorption of a material.

Figure 9. Digital photo of the DSC instrument used in this research

2.7.11 Tensile strength measurement

The tensile strength test was performed using an Instron 3367 following the ASTM D882-97 Standard. The specimens were films with dimensions of 50 mm of length, 10 mm of uniform width, and thickness of around 2.45 mm. The test was performed at a rate of 10 mm/min.

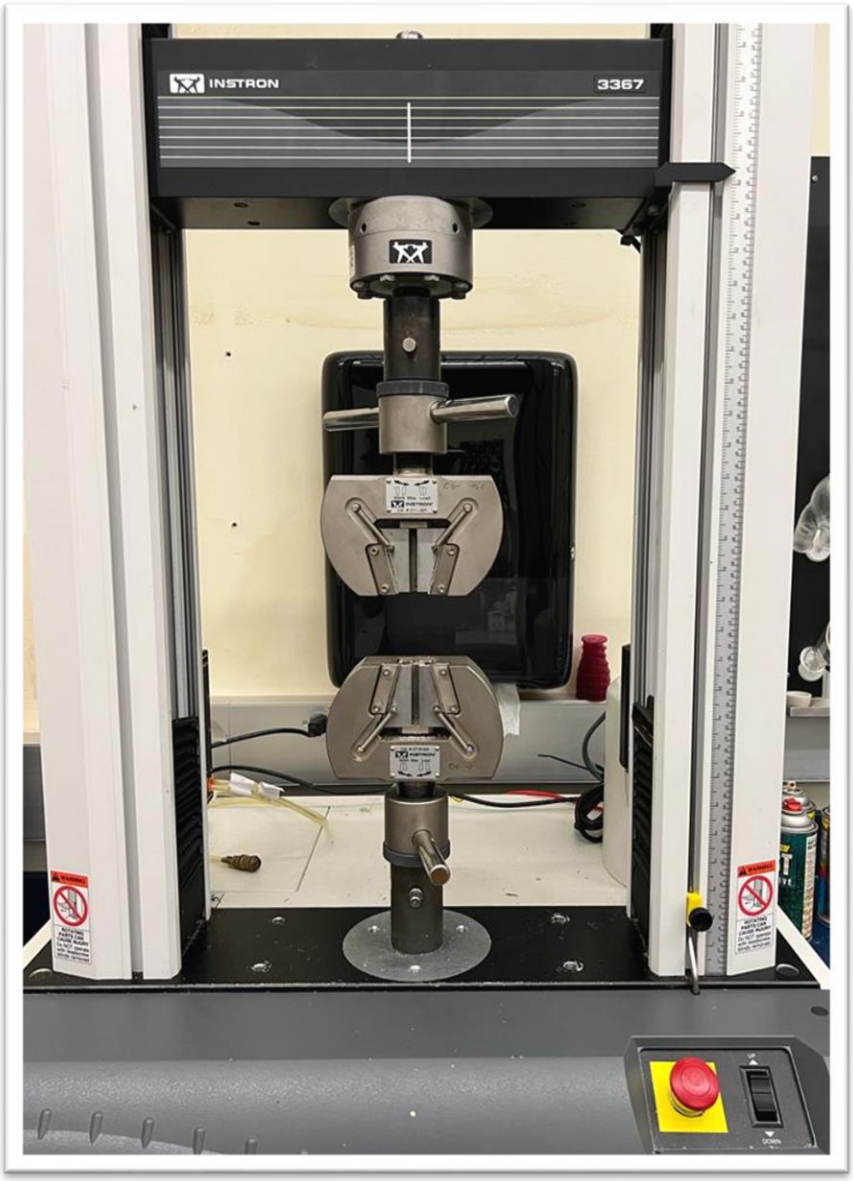

Figure 10. Digital image of the tensile strength instrument used in this research

2.7.12 Contact angle

In material characterization, the water contact angle (WCA) is frequently employed, particularly for polymers, coatings, and thin films. This information is deemed crucial for understanding how a material will interact with liquids in practical applications. The investigation of surface energy and wettability using WCA instruments involves measuring the contact angle of a specific chemical droplet on a surface, allowing the determination of the material's hydrophobic or hydrophilic nature. This combined approach provides a comprehensive understanding of the material's surface properties, aiding in the design and optimization of materials for various applications. The WCA was measured by using an Ossila Contact Angle Goniometer. Every analysis was performed at least twice.

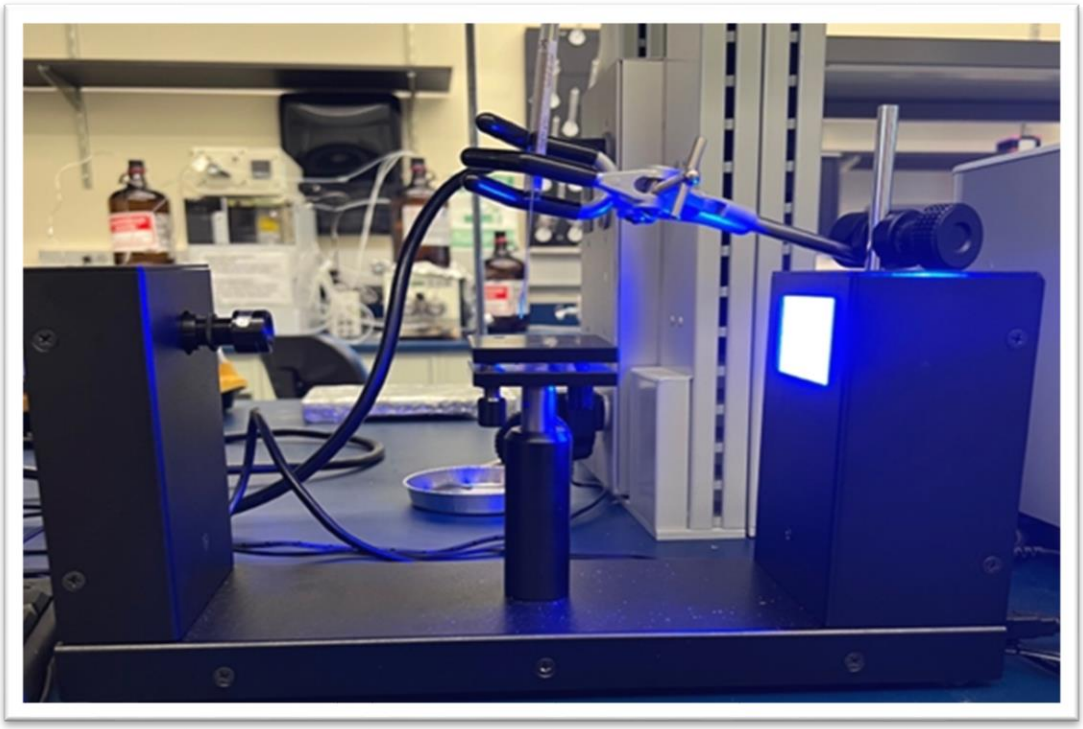

Figure 11. Digital image of contact angle instrument used in this research

2.7.13 Degree of swelling and gel content

The degree of swelling gives information regarding a polymer's capability to absorb and retain a solvent; however, the gel content is the insoluble fraction of a cross-linked polymer. In addition, the degree of swelling test involves immersing a cured adhesive sample in a solvent for a specific period. After the immersion, the swollen samples are weighed, and the degree of swelling is calculated as the weight of the swollen sample increased as compared to the initial dry weight of the sample.

The gel content test assesses the extent of cross-linking in a cured adhesive. This test was performed with a cured adhesive sample when samples were dissolved in a solvent to extract the soluble components. The remaining insoluble gel fraction is then dried in an oven for 48 hours and weighed. The percentage of gel content was calculated with the original weight of the sample and dried weight after extraction.

CHAPTER III

RESULTS AND DISCUSSION

3.1 Fourier transform infrared spectra of castor oil, epoxidized castor oil, and castor oil polyol

Figure 12a represents the FT-IR spectra of CO, ECO, and COP to determine the characteristics of the functional group present in the materials. The stretching vibration of C=C and stretching vibration of alkene C-H (=C-H) of CO was confirmed by the peaks that appeared at 1650 cm^{-1} and 3004 cm^{-1} respectively [20], which are found to disappear in the IR spectra of ECO after epoxidation reaction, and a new peak was recorded at about 843 cm^{-1} due to the presence of epoxide group (C-O-C) in ECO [20]. It indicates that the double bond of CO is successfully modified into epoxide. Also, the peak around 3400 cm^{-1} in the IR spectra of CO shows the presence of naturally available hydroxyl group (O-H) in the structure of CO. Moreover, after the ring-opening reaction, in the IR spectra of COP, the peak intensity for the stretching vibration of O-H is observed to be increased suggesting a successful ring-opening reaction [20]. The FT-IR spectra therefore validated the chemical alteration of the COP from the CO via epoxidation and ring-opening reaction [21].

3.2 Gel permeation chromatography of castor oil, epoxidized castor oil and castor oil polyol

After the successful formation of ECO and COP, the samples were characterized by GPC to monitor the reaction progress using finding molecular weight (**Figure 12b**). The polymeric beads that make up the stationary phase have larger pores so that larger molecules can pass through them without being trapped. However, due to the porosity in the stationary phase, smaller molecules take longer to move through the column. The retention time for CO and COP is observed at almost similar position which is 32.13 and 32.11 respectively as they both contain hydroxyl group but, it is lower than ECO due increase in the hydrogen bonding in COP. The increased hydrogen bonding will result in increasing intermolecular forces thus increasing viscosity and molecular weight of COP. In addition, a shoulder appeared at the retention period around 30.40 min, which may have resulted from dimers formed as a byproduct of the reaction from ECO to COP [21].

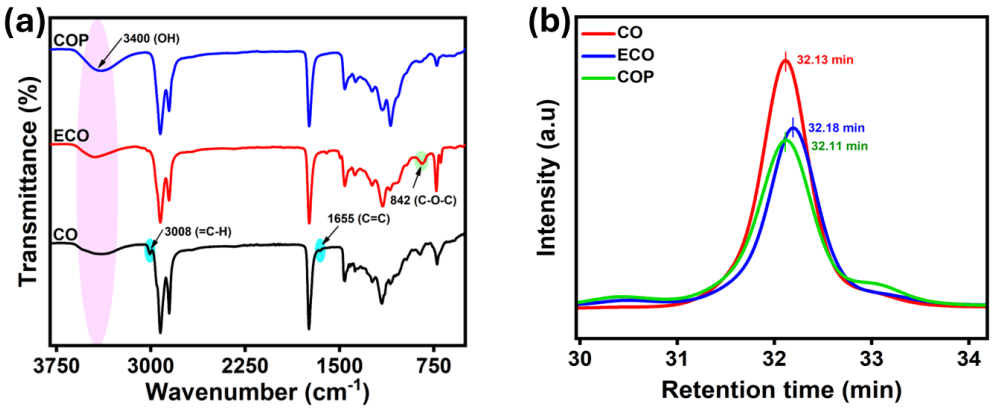

Figure 12. (a) FT-IR, and (b) GPC spectra of CO, ECO, and COP

3.3 Fourier transform infrared spectra of chain extenders

The synthesis of the chain extenders (ETP and ETAM) from their monomers (DTD, DTP, and EA) was confirmed by the FT-IR spectra (**Figure 13**). **Figure 13a** represents

the FT-IR spectra of the DTD synthesized using 2,5-TDCA. It can be seen from the spectra that the peak of -C=O of the carboxylic acid group at 1655 cm^{-1} is found to be shifted to 1714 cm^{-1} indicating the -C=O of the ester group [22]. The peak for -OH stretching vibration of carboxylic acid group is observed at 2965 cm^{-1} and 3095 cm^{-1} in 2,4-TDCA [23]. Also, the two new peaks were observed at 1103 cm^{-1} and 1262 cm^{-1} confirming the formation of C-O-C linkage. Thus, it can be concluded that DTD is successfully synthesized. Spectra in the range of 2830-3009 cm^{-1} were recorded for the symmetric and asymmetric -CH stretching vibration in the starting materials (DTD and DTP) [24], which was also observed in the final synthesized product. Interestingly the spectra of DTD and DTP were nearly identical to each other. In addition, the peak for the carbonyl group (C=O) observed at 1714 cm^{-1}, in starting materials DTD and DTP, was found to shift to 1620 cm^{-1} and 1621 cm^{-1} in final products confirming the amide carbonyl linkage (-CONH) [25]. Whereas the peaks for the C-O-C linkage at 1262 cm^{-1} and 1103 cm^{-1} disappeared in the final products (ETP and ETAM), indicating the successful synthesis of ETP and ETAM. Moreover, two peaks for the primary amine group of EA between 3200-3300 cm^{-1} were successfully converted into the secondary amine which appeared around 3290 cm^{-1} in both the final products. Also, the peak for the hydroxyl group of EA was observed around 3400 cm^{-1} in both the final products (ETP and ETAM) [26,27].

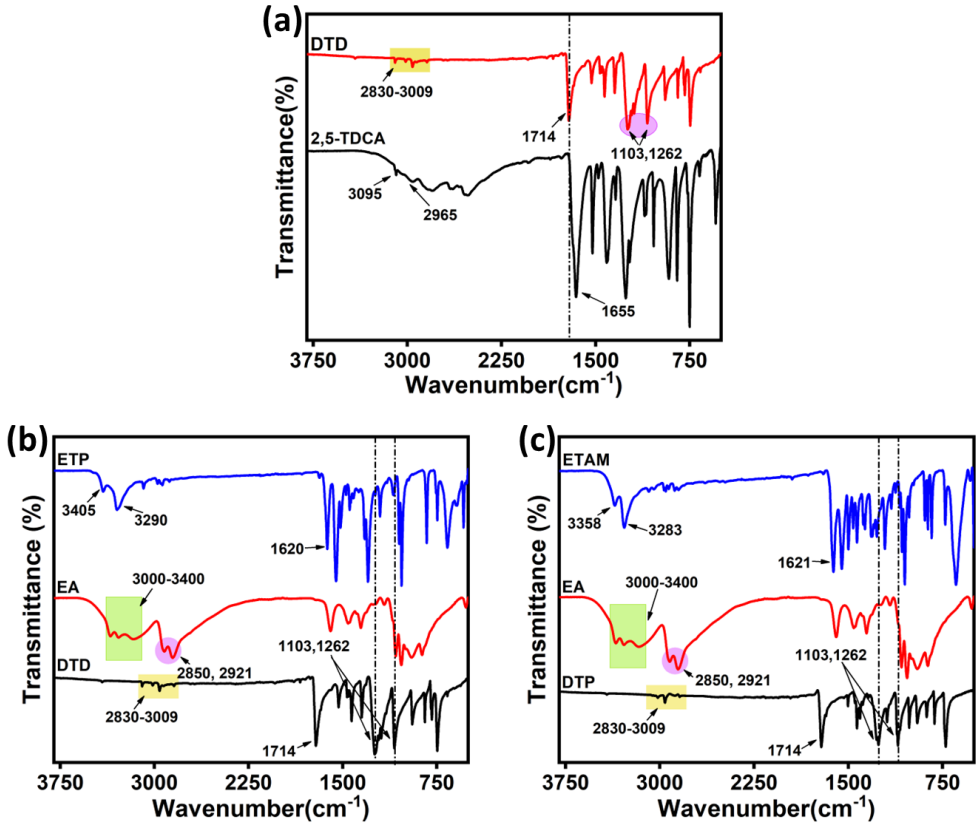

Figure 13. FT-IR of synthesized (a) DTD, (b) ETP, and (c) ETAM compounds

3.4 ^{1}H Nuclear magnetic resonance of chain extenders

The synthesis of the compounds (DTD, ETP, and ETAM) was also confirmed with the NMR spectra (**Figure 14**). The signal at 2.37 ppm and 3.19 ppm indicates protons of dimethyl sulfoxide (DMSO) and water. The protons of the terminal methylene group present in DTD were observed at 3.72 ppm in **Figure 14a.** In all the samples the protons of the aromatic methylene group were observed at 7.59 ppm (labelled as in **Figure 14a-c),** whereas the protons of methylene group of the aliphatic chain were found to be at 3.24 and 3.41 ppm (labelled as b & c in **Figure 14b & c).** The protons of the hydroxyl group and amide group were observed at 4.68 and 8.47 ppm (labelled as d & e in **Figure**

14b & c) [28]. Thus, NMR spectra confirm the successful synthesis of all the compounds.

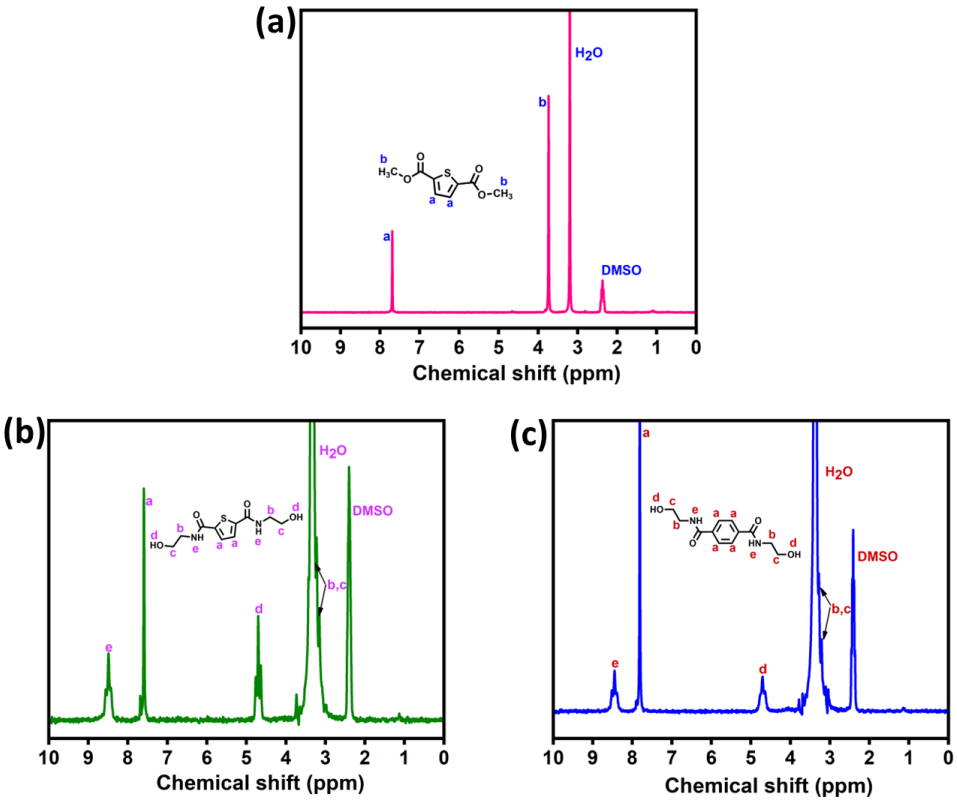

Figure 14. NMR spectra of synthesized (a) DTD, (b) ETP, and (c) ETAM compounds

3.5 Fourier transform infrared spectra of PU adhesives

Figure 15 displays the FT-IR spectra of the prepared adhesive samples that contained the two synthetic chain extenders. The reaction takes place between two reactive groups (OH and NCO), where diisocyanates react with two OH groups, one of COP and the second one of the OH group of cross-linkers (ETP or ETAM). The hydroxyl group observed at 3420 cm^{-1}, in COP, has vanished and the spectra observed at 3328 cm^{-1} indicate the -NH group of urethane moieties in the adhesive samples. Strong peaks at 1215 cm^{-1} due to C-N stretching vibration, 1523 cm^{-1} for N-H bending, and 1726 cm^{-1} for CO-NH stretching confirm the formation of urethane group in adhesives [29].

Moreover, a peak around 2270 cm^{-1} in final products indicates the isocyanate group (N=C=O) which was found unreacted in the adhesive samples [30–32]. However, the FT-IR spectra of all the adhesive samples with increasing wt.% of chain extenders (ETP and ETAM) showed decreasing peak intensity of the isocyanate group in the adhesive samples.

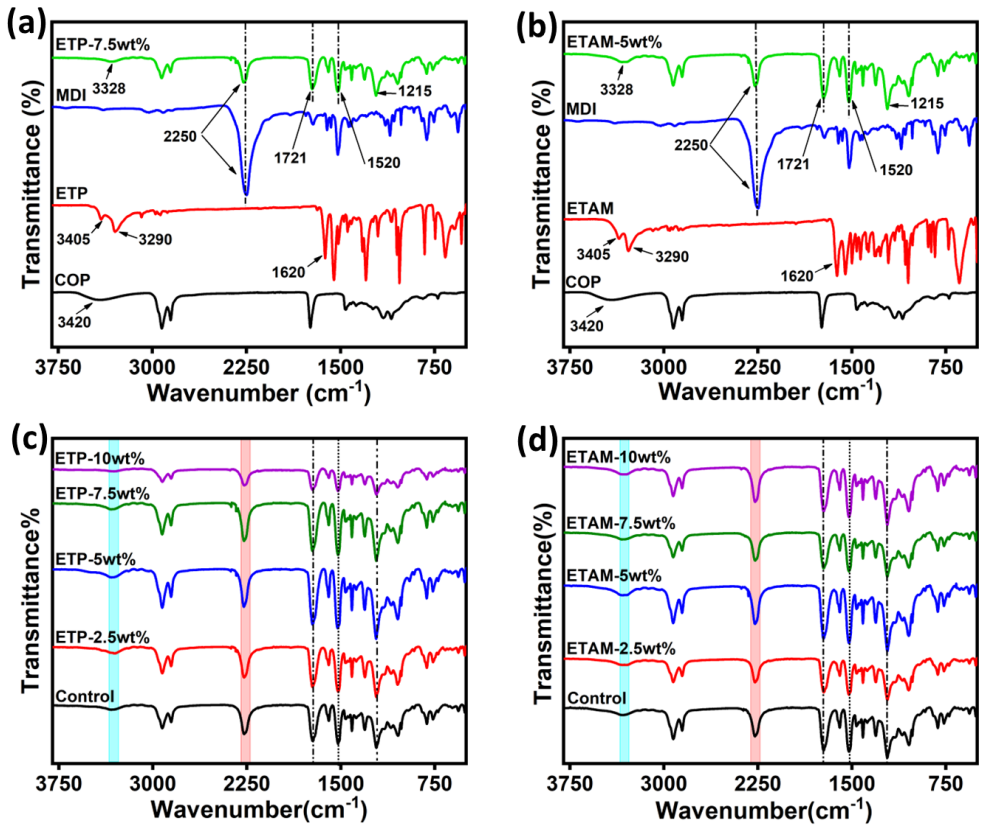

Figure 15. FT-IR spectra of (a) & (b) comparison of ETP-7.5 wt.% and ETAM-5 wt.%, respectively with monomers, (c) & (d) varying wt.% of ETP and ETAM, respectively in PU adhesive samples

3.6 Tensile strength

In tensile testing, the mechanical properties of the adhesive samples were evaluated using two distinct crosslinkers. The mechanical properties of the adhesive were found to be changed noticeably as the amounts of crosslinkers varied (**Figure 16**). To evaluate

the bonding capabilities, the adhesive was mixed with varying weight percentages of ETP and ETAM. The tensile strength of the control sample was 5.10 MPa without any chain extender. There is an increasing trend in tensile strength up to 7.5 wt.% in ETP and 5 wt.% in ETAM adhesives. The adhesive sample with 7.5 wt.% ETP cross-linker exhibited the highest bonding strength of 7.22 MPa compared to all the samples with ETP as chain extender; however, with 10 wt.% ETP, the bonding strength dropped to 6.99 MPa. Moving forward to the adhesive samples that contain ETAM chain extender, 5 wt.% ETAM incorporation gives the highest tensile strength (9.68 MPa), whereas loadings of 7.5 wt.% and 10 wt.% ETAM, respectively reduce this strength to 8.86 MPa and 8.29 MPa which is due to optimal crosslinking of the polymeric material after increasing the chain extender of a certain weight percentage (5 wt.% for ETP and 7.5 wt.% for ETAM). Most interestingly, the higher incorporation of a chain extender led to a more rigid and brittle structure, reducing the material's ability to absorb stress, and resulting in lower tensile strength, this may be a reason behind the decreasing trend in mechanical strength. Also, the bonding strength on stainless steel metal coupons was tested using three different weight percentages (5, 7.5, and 10 wt.%) of adhesive samples with both chain extenders. The bar graph illustrates that, compared to the bonding strength of 7.5 wt.% and 10 wt.% incorporation, 5 wt.% of ETP and ETAM crosslinkers on metal coupons display promising results with 6.18 MPa and 6.73 MPa, respectively. On top of it, these results are compared with some other published work in **Table 5**. As seen in this table, samples prepared in this study showed improved adhesive properties.

Table 5. Comparison of mechanical strength with other published bio-based polymeric materials

Sr. No	Bio-based material	Fillers	Substrate	Tensile Strength (MPa)	Ref.
1	Castor Oil	Cellulose Acetate	Poplar wood	2.84	[32]
2	Castor oil	Cadaverine + Nvoc-Cl	Polyethylene	4.6	[33]
3	Castor oil	Cadaverine + Nvoc-Cl	Oak wood	2	[33]
4	Soy protein	CNF-CA	Poplar wood	8.42	[34]
5	Soy protein	Undecylenic acid	Cherry wood	6.67	[35]
6	$NaHSO_3$ modified soy protein	-	Cherry wood	6.18	[36]
7	$NaHSO_3$ modified soy protein	Extruded Sorghum lignin	Cherry wood	5.94	[36]
8	$NaHSO_3$ modified soy protein	Sorghum lignin	Cherry wood	5.7	[36]
9	Soluble fraction of soy flour	--	Maple veneers	6.8	[37]
10	Soluble fraction of soy flour	Magnesium oxide	Maple veneers	7.5	[37]
11	Soy protein isolate	Magnesium oxide	Maple veneers	9.1	[37]
12	Insoluble carbohydrates of soy flour	Magnesium oxide	Maple veneers	3.4	[37]
13	Lignin	Formaldehyde	Hard wood	4	[38]
14	Lignin	Glyoxal	Hard wood	3.9	[38]
15	Hyperbranched polyacid	Xylitol + Maleic anhydride	Plywood	2.37	[39]
16	Palm oil-based polyester polyol	Glycerol	Teak wood	5.3	[40]
17	Palm oil polyol	-	Hard wood	2.6	[41]
18	Jatropha oil polyol	-	Hard wood	4.9	[41]

19	Canola polyol	-	Birch wood	5.7	[42]
20	Tree bark	-	Aspen wood	3.5	[43]
21	Microcryatalline cellulose	-	Hard wood	5.47	[44]
22	Sawdust	-	Hard wood	5.36	[44]
23	Castor Oil	-	Wood	2.19	[45]
24	Tannin	HBPA	Plywood	1.37	[46]
25	High temperature soybean meal	Plyamidoamine epichlorohydin	Plywood	2.6	[47]
26	Soy protein isolate	Furfuryl alcohol, Phytic acid	Poplar plywood	1.61	[48]
27	Dialdehyde cellulose	Polyamine	Poplar wood	3.29	[49]
28	Methacrylate-function-alizedsoybeanoil	Allyl urea	Steel	1.76	[50]
29	Castor Oil	-	Pinewood	1.9	[31]
30	Tannin/hexamine	-	Poplar plywood	0.99	[51]
31	Tannin/hexamine	Boric acid	Poplar plywood	1.78	[51]
32	Soya flour	Nano Cross-linker	Plywood	2.94	[52]
33	Epoxidized soybean oil	Urea-formaldehyde	Plywood	1.88	[53]
34	Epoxidized starch	Bisphenol A, Epichlorohydrin	Birch wood	4.5	[54]
35	Camelina protein	Ultrasound driven lignin	Pine wood	2.45	[55]
36	Regenerated silk	Tannin, Furfuryl alcohol	Plywood	3.2	[56]
37	Soyproteinisolate (SPI)	CPA, TGA	Plywood	1.83	[57]
38	Poly(ε-caprolactone-co-lacticacid)	-	Polycarbonate	8.85	[58]
39	Isolated soybean protein (SPI)	Tannin, Sucrose	Plywood	1.5	[59]
40	Soybean meal	Pulp Fiber	Plywood	1.78	[60]
41	Soybean meal	Poplar wood fibre	Plywood	1.32	[60]
42	Soybean meal	Bagasse fibre	Plywood	1.23	[60]

43	COP	ETP	Oak wood	7.22	[This work]
44	COP	ETAM	Oak wood	9.68	[This work]

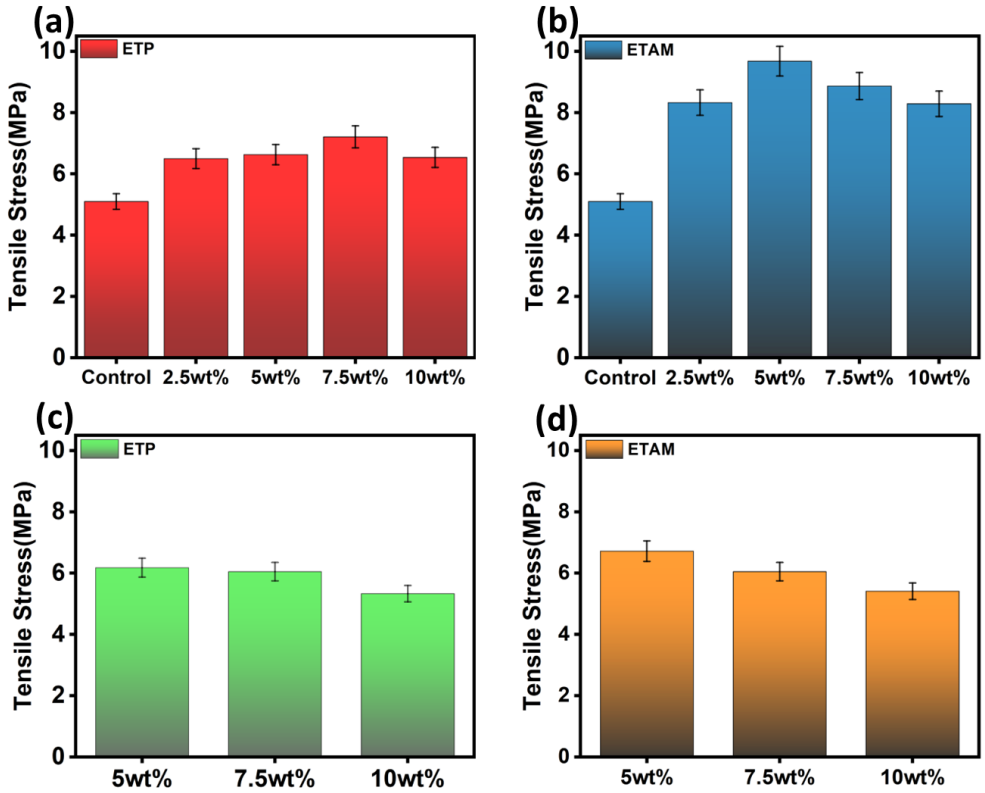

Figure 16. Tensile strength of (a) different wt.% of ETP in PU adhesive (b) different wt.% of ETAM in PU adhesive (c) different wt.% of ETP in PU adhesive on steel coupon (d) different wt.% of ETAM in PU adhesive on steel coupon

3.7 Thermogravimetric analysis

By comparing the TGA and DTG curves, the thermal decomposition behavior of adhesives, with varying chain extender concentrations, under the nitrogen atmosphere, can be determined (**Figure 17**). With increasing wt.% of chain extenders (ETP & ETAM) in the polymeric material the thermal decomposition temperature was observed to be in decreasing trend which could be due to the rigid network structure promoted

by the chain extenders while reducing its flexibility. Moreover, the higher concentration of chain extenders may result in higher crosslink density in a polymeric network which is responsible for forming brittle polymer that might not withstand high thermal stress. Sample weight loss of 5% and 30% at decomposition temperatures ($T_{5\%}$ and $T_{30\%}$), maximum decomposition rate (T_{MAX}), heat resistance index temperature (T_{HRI}), glass transition temperature (Tg), and residual mass in wt.% are displayed in **Table 6**. T_{HRI} value is calculated using **equation 1** [41].

$$T_{HRI} = 0.49[T_{-5\%} + 0.6(T_{-30\%} - T_{-5\%})] \quad (1)$$

Table 6. Comparison data of $T_{5\%}$, $T_{30\%}$, T_{MAX}, T_{HRI}, Tg and Residual mass

Sample name	$T_{5\%}$	$T_{30\%}$	T_{MAX} (%)	T_{HRI}	Tg (ºC)	Residual Mass (%)
Control	293	359	458	162	88	6.26
ETP-2.5wt%	286	355	452	160	95.10	6.28
ETP-5wt%	286	354	451	160	98.55	7.05
ETP-7.5wt%	283	352	451	158	101.52	6.50
ETP-10wt%	277	344	450	155	103.92	2.99
ETAM-2.5wt%	288	356	450	161	96.14	6.65
ETAM-5wt%	281	352	454	158	100.87	6.81
ETAM-7.5wt%	274	350	453	156	101.92	6.90
ETAM-10wt%	271	350	454	156	102.72	6.40

Each adhesive shows thermal degradation in two stages. In the first stage, larger PU molecules are broken down into polyol and isocyanate between the 200 ºC to 400 ºC temperature range. Including the control sample, all the samples exhibit two

degradation peaks between 200 ºC and 400 ºC on the derivative thermogram (DTG) graph. In which the degradation from 250 ºC to 350 ºC could be due to the dissociation of small or unreacted molecules whereas from 350 ºC to 400 ºC is ascribed to the dissociation of larger molecules. Further molecular dissociation of polyol and isocyanate or the decomposition of char residues which are formed in the previous phase has occurred during a second thermal breakdown between 400 ºC and 500 ºC [32]. As compared with the control sample the intensity of degradation peaks is found to decrease with the addition of chain extenders which indicates good thermal stability of the adhesive samples.

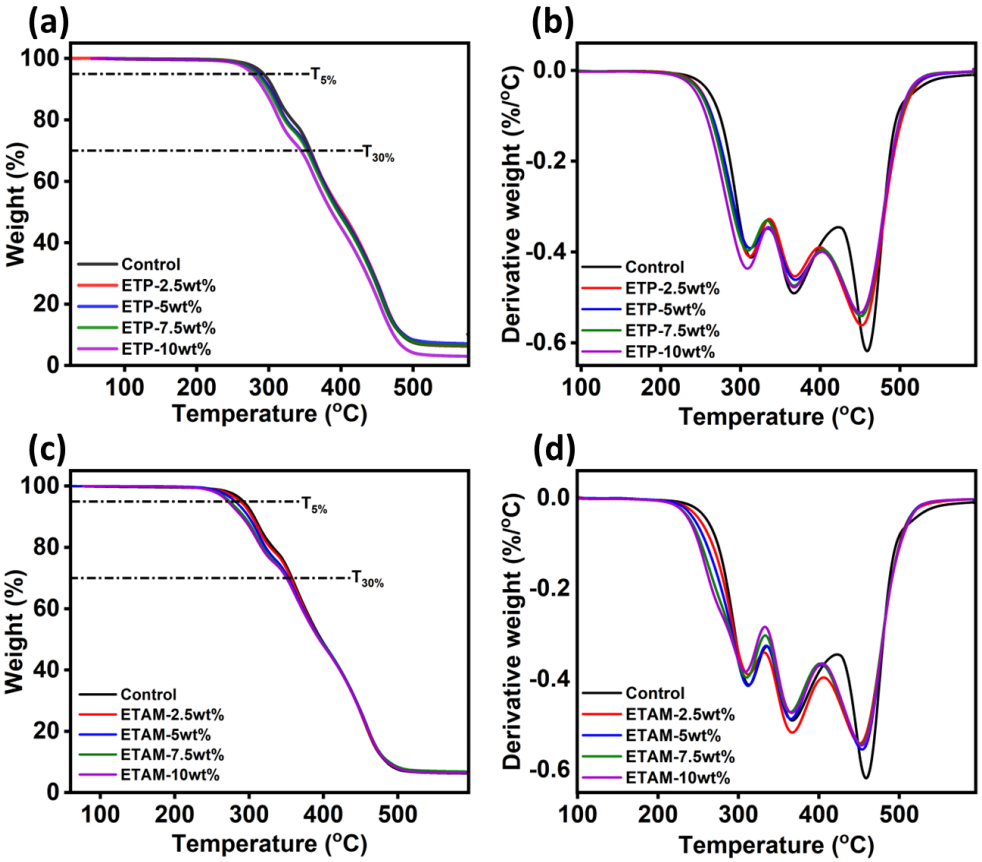

Figure 17. TGA and DTG of (a & b) PU adhesives with varying wt.% of ETP, and (c & d) PU adhesives with varying wt.% of ETAM

3.8 Differential scanning colorimetry

DSC graphs indicate the thermal transition temperature of all the adhesive samples which was synthesized by adding two different crosslinkers in the increasing order of wt.% (**Figure 18**). The temperature range for all the experiments was from -50 ºC to 200 ºC, with a ramp rate of 10ºC/minute. For all the samples, the glass transition temperature (T_g), indicating an endothermic process, is found to increase in Tg temperature with increasing wt.% of cross-linkers as shown in **Table 6**. The T_g for the control sample is found at 88 ºC which is found to increase to 103.92 ºC and 102.72 ºC for the highest incorporation of ETP and ETAM crosslinkers respectively. As the concentration of chain extender rises, more cross-links form between polymer chains. The increased cross-linking may restrict the molecular mobility of the polymer, leading to higher Tg values.

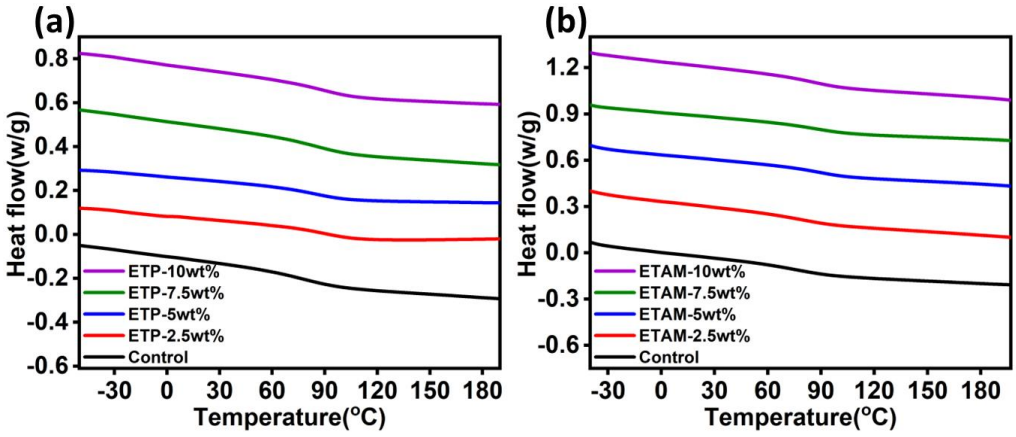

Figure 18. Differential scanning calorimetry (DSC) of (a) PU adhesives with varying wt.% of ETP (b) PU adhesive with varying wt.% of ETAM

3.9 Gel content and degree of swelling

Gel content refers to the percentage of polymer chains that undergo crosslinking and remain insoluble in a certain solvent, providing information on the level of crosslinking in the polymer structure. Increased gel content indicates more crosslinking, which is

usually associated with improved mechanical properties and thermal resistance. This characteristic is crucial in adhesive applications, where structural strength and dimensional stability play a vital role. Whereas the extent of swelling indicates the polymer network's ability to absorb and hold solvent molecules which in turn shows its crosslink density. Greater swelling suggests a more open and flexible polymer structure, whereas reduced swelling might imply a more compact network, thus enhancing mechanical durability. Thus, both tests were performed with the best tensile strength showing adhesive samples (ETP 7.5 wt.% and ETAM 5 wt.%). Adhesive samples were immersed in nine different solvents based on polar aprotic solvents THF, N-methyl-2-pyrrolidone (NMP), dimethyl formamide (DMF), DMSO, and acetone), polar protic solvents (water, methanol, and ethanol) and non-polar solvent (toluene) for 24 h (**Figure 19**). After that, the samples were dried in an oven at 75 ºC for 48 h (**Figure 20**). The swelling capacity of a polymer is closely related to its degree of crosslinking and its interaction with a solvent. If a crosslinked polymer and solvent exhibit favorable interactions, the polymer will often experience more swelling. This underscores the significance of intermolecular interactions at the molecular level in determining the extent of swelling of a polymer when in contact with a solvent. The degree of swelling (DS) can be calculated through **Equation 2**.

$$DS\ (\%) = \frac{m_1 - m_0}{m_0} \times 100 \quad (2)$$

Where $m_0$the initial is weight and m_1 is the weight after swelling. However, a portion of the polymer undergoes dissolution, which is subsequently eliminated from the polymer structure during drying. This phenomenon results in a decrease in the polymer's mass compared to its initial weight prior to swelling, enabling the determination of gel content using **Equation 3.** Where m_2 is the weight after drying.

$$GC\ (\%) = \frac{m_2}{m_0} \times 100 \quad (3)$$

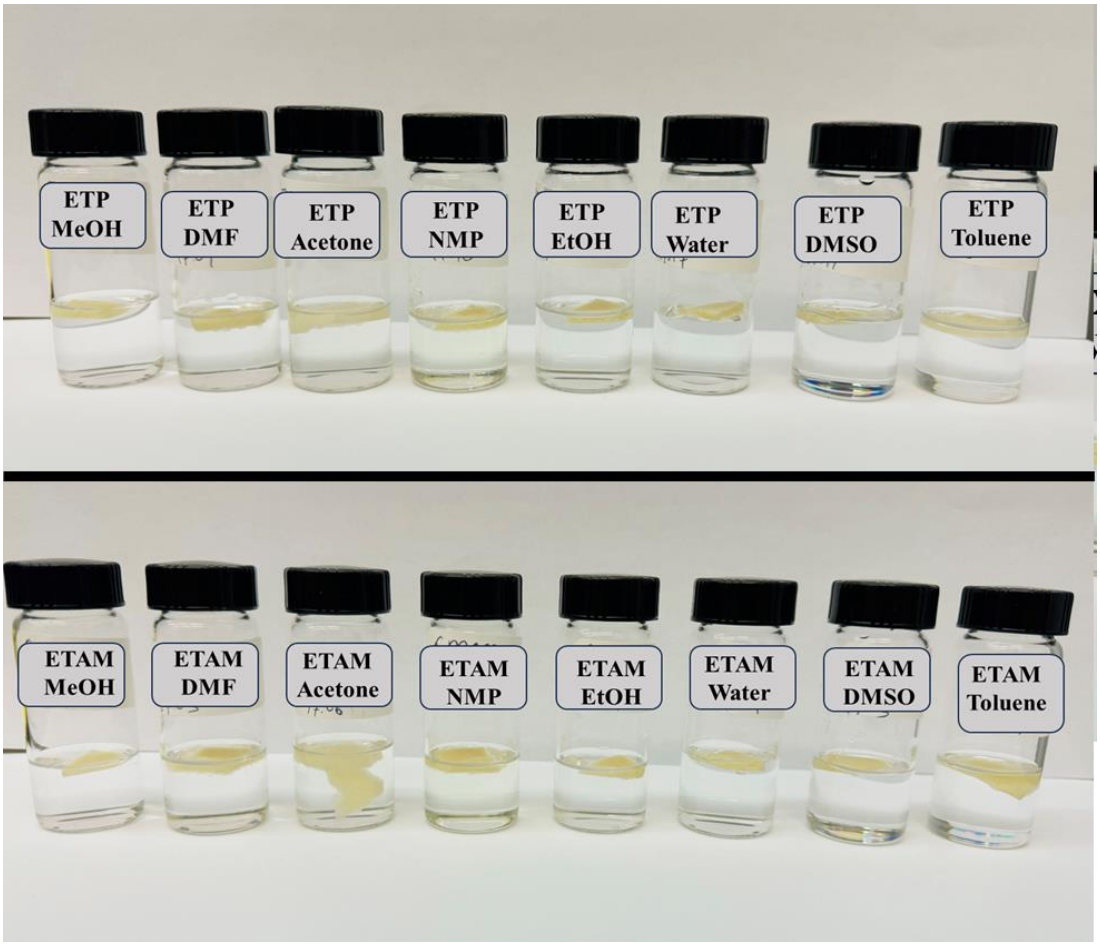

Figure 19. ETP-7.5 wt.% and ETAM-5 wt.% in nine different solvents for 24 h for gel content and degree of swelling

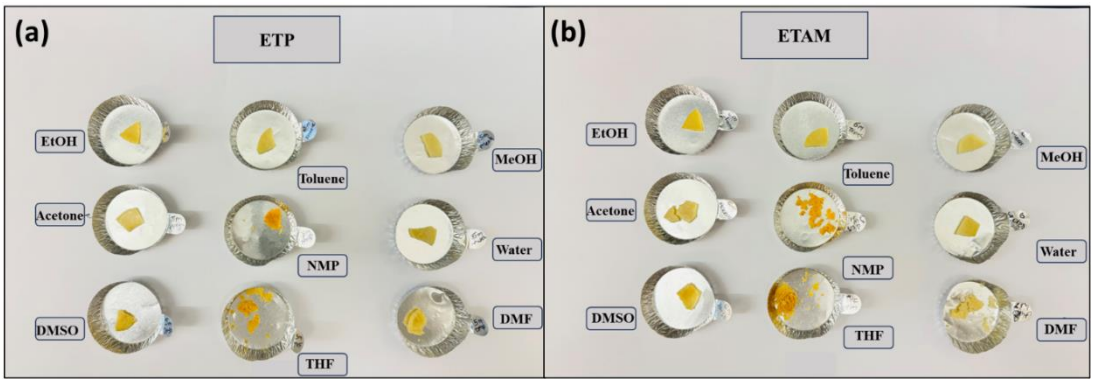

Figure 20. Dried samples of ETP-7.5 wt.% and ETAM-5 wt.% in oven at 70 ºC for 48 h after putting into nine different solvents

Figure 21a shows the gel content of the two best polymeric materials from all the synthesized adhesive samples. From the **Figure 21**, it is observed that for non-polar solvent's (toluene) gel percentage is equal (94 %) for both materials (ETP 7.5 wt.% and ETAM 5 wt.%) because COP-based polymeric materials contain polar functional group whereas, non-polar nature of toluene might not dissolve the adhesive material, so it has not only higher gel content but also same gel percentage. While in NMP, DMF, and acetone, gel percentage is 77%, 87%, and 90%, respectively for ETP-containing PU adhesive which is lower than ETAM PU adhesive material for the same solvents which means the ETAM adhesive sample indicates a higher degree of cross-linking or network formation within the polymer structure than ETP containing PU material which can be correlated with its tensile strength as well as it has higher tensile strength than ETP. That means higher cross linkage replicates good bonding strength and this how tensile strength would be higher. At first glance, ETAM has higher gel content as compared to ETP in most of the polar aprotic solvents whereas it is almost the same for polar protic and non-polar solvents because of less solubility of polar groups of adhesive material in polar protic and non-polar solvents. Interestingly, ETP-containing PU and ETAM-containing PU samples have shown almost 100% gel content in water, DMSO, methanol, and ethanol which means no degradation happened in these solvents. These two samples have shown more than 85% gel content in all the solvents except two solvents (THF and NMP). Overall, a higher gel percentage suggests increased cross-linking, which leads to good mechanical strength which is also observed in tensile strength as well.

Figure 21b represents the degree of swelling of the best tensile strength showing adhesive materials. For polar protic solvents, samples in water have shown less than 50% swelling because these two materials might be hydrophobic. While in methanol

and ethanol, both the samples have shown at almost 100%. ETAM containing PU has shown a 600% degree of swelling in NMP which is the highest among all the solvents, same as ETP containing PU has shown a 470% degree of swelling in the same solvent which is second highest in all the solvents. Importantly, ETAM containing PU has shown less swelling in THF, DMF, toluene, water, and ethanol and is almost equal in acetone, water, DMSO, and methanol which means ETAM has shown less swelling as compared to ETP. Which indicates that less swelling replicates higher cross-linkage. This phenomenon is also confirmed by the gelling percentage of ETAM material. So, ETAM is higher cross-linked material among all which is why it has the highest tensile strength (ETAM-5 wt.% - 9.68MPa) among all the synthesized adhesive materials. After removing the samples from solvents and drying them in an oven at 75 °C for 24 h.

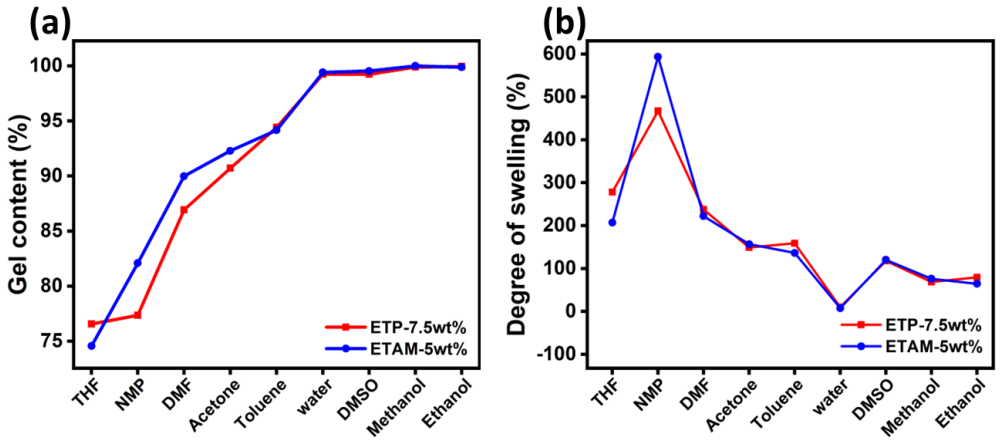

Figure 21. Percentage of gel content (a) and swelling degree (b) of ETP-7.5 wt.% and ETAM-5 wt.% in different solvents

3.10 Contact angle

The surface tension of a solid can be determined with the use of an Ossila Contact Angle Goniometer by measuring the angle formed between the solid and a droplet of liquid resting on the surface. When describing the relative affinity of water molecules to

spreading on the surface of any substrate, the words hydrophilicity ($\theta < 90^o$) and hydrophobicity ($\theta > 90^o$) are used [61]. The contact angles for the ETP and ETAM samples were performed with three different solvents which are water, glycerol, and ethylene glycol (EG) (**Figure 22**). The average contact angle for the ETAM sample was found to be 98.51º and for the ETP sample to be 112.56º for the water **(Figure 22c & f)**. The adhesive materials were found to be hydrophobic since their contact angles were greater than 90º for water. In addition, the contact angle consistently decreased as the solvent polarity decreased in the glycerol **(Figure 22b & e)** and EG **(Figure 21a & d)** sequences.

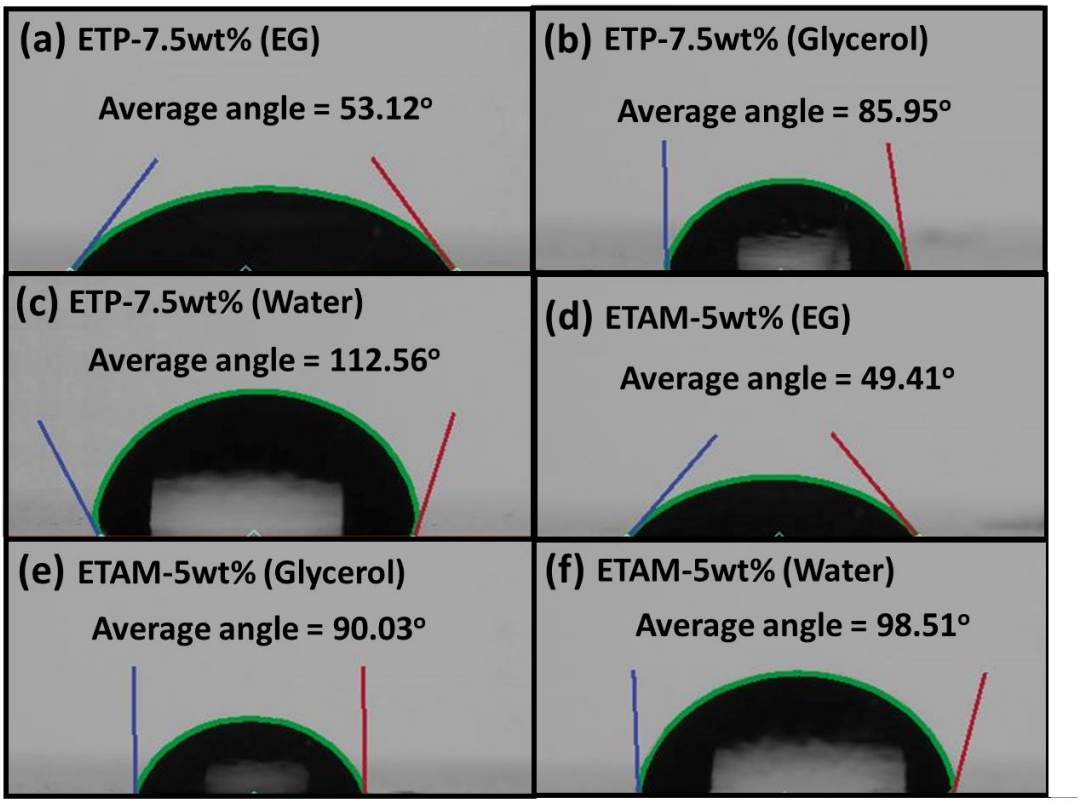

Figure 22. Contact angle of (a-c) ETP-7.5 wt.% and (d-f) ETAM-5 wt.% adhesive samples with EG, glycerol, and water

CHAPTER IV

CONCLUSION

In this work, novel adhesives were successfully synthesized by using bio-based COP and chain extender for exceptional mechanical strength. After increasing the weight percentage of the chain extender, tensile strength was increased at 9.61 MPa of ETAM adhesive material, and mechanical strength was also good on metal coupons (6.73 MPa). This is due to the additional cross-linking of chain extenders which is almost higher than other renewable source-based adhesives in this article. So, this material is competitive and better to replace petroleum-based polyols. Meanwhile, a trend in DSC graphs revealed a significant correlation between the incorporation of crosslinkers and the glass transition temperature in adhesive samples. Higher concentrations of ETP and ETAM crosslinkers led to increased Tg temperatures, indicating enhanced cross-linking and reduced polymer mobility. This suggests a direct influence of crosslinker concentration on the thermal transition behaviour of the synthesized adhesives. Both materials display excellent stability in water, DMSO, methanol, and ethanol. ETAM adhesive's lower swelling and higher gel content contribute to its superior tensile strength (9.68 MPa) compared to ETP adhesives. These results emphasize the crucial role of cross-linking in determining adhesive material properties. The adhesive samples incorporating ETP and ETAM crosslinkers exhibited hydrophobic behaviour, as indicated by contact angles exceeding 90º in water so, the hydrophobic nature of the adhesive materials makes them better to use in kitchen furniture.

CHAPTER V

FUTURE WORK

In this study, isocyanate was employed to create urethane linkages. However, for the synthesis of non-isocyanate polyurethane (NIPU), the terminal hydroxyl (-OH) groups of the diols can be replaced by reacting these diesters with diamines, such as ethylene diamine. The chain length of these diamines can be varied to explore different properties and performance characteristics. Additionally, both cyclic and aromatic diamines can be utilized in the synthesis of NIPU adhesives. This variation allows for the investigation of how different diamine structures influence the adhesive properties. For instance, the use of cyclic and aromatic diamines could enhance rigidity and thermal stability, they might improve the mechanical strength and chemical resistance of the adhesives as well. Furthermore, the EA component can be substituted with other chain length having NH_2 and OH terminal groups. By altering the carbon chain length, researchers can study the effects on the adhesive properties, such as flexibility, tensile strength, and durability. This approach enables a comprehensive understanding of how molecular modifications impact the overall performance of NIPU adhesives, potentially leading to the development of tailored adhesives for specific applications. Overall, this isocyanate-based study can be replaced as NIPU.

REFERENCES

[1] H. Dodiuk, Handbook of thermoset plastics, William Andrew, 2021.

[2] J.O. Akindoyo, M.D.H. Beg, S. Ghazali, M.R. Islam, N. Jeyaratnam, A.R. Yuvaraj, Polyurethane types, synthesis and applications-a review, RSC Adv. 6 (2016) 114453–114482.

[3] F.M. De Souza, P.K. Kahol, R.K. Gupta, Introduction to Polyurethane Chemistry, ACS Symp. Ser. 1380 (2021) 1–24.

[4] J.O. Akindoyo, M.D.H. Beg, S. Ghazali, M.R. Islam, N. Jeyaratnam, A.R. Yuvaraj, Polyurethane types, synthesis and applications-a review, RSC Adv. 6 (2016) 114453–114482.

[5] A. Delavarde, G. Savin, P. Derkenne, M. Boursier, R. Morales-Cerrada, B. Nottelet, J. Pinaud, S. Caillol, Sustainable polyurethanes: toward new cutting-edge opportunities, Prog. Polym. Sci. (2024) 101805.

[6] M. Zieleniewska, M. Auguścik, A. Prociak, P. Rojek, J. Ryszkowska, Polyurethane-urea substrates from rapeseed oil-based polyol for bone tissue cultures intended for application in tissue engineering, Polym. Degrad. Stab. 108 (2014) 241–249.

[7] D.A. Babb, Polyurethanes from renewable resources, Adv. Polym. Sci. 245 (2012) 315–360.

[8] B. Müller, W. Rath, Formulierung von Kleb-und Dichtstoffen: das kompetente Lehrbuch für Studium und Praxis, Vincentz Network GmbH & Co KG, 2004.

[9] G. Habenicht, Kleben: Leitfaden für die praktische Anwendung und Ausbildung, Springer-Verlag, 2013.

[10] A. Pizzi, K.L. Mittal, Handbook of adhesive technology, CRC press, 2017.

[11] F. Ferdosian, Z. Pan, G. Gao, B. Zhao, Bio-based adhesives and evaluation for

wood composites application, Polymers (Basel). 9 (2017).

[12] A. Manuscript, Green Chemistry, (2019).

[13] E.F. Gómez, F.C. Michel, Biodegradability of conventional and bio-based plastics and natural fiber composites during composting, anaerobic digestion and long-term soil incubation, Polym. Degrad. Stab. 98 (2013) 2583–2591.

[14] D.P. Pfister, Y. Xia, R.C. Larock, Recent advances in vegetable oil-based polyurethanes, ChemSusChem. 4 (2011) 703–717.

[15] S.A. Madbouly, Y. Xia, M.R. Kessler, Rheological behavior of environmentally friendly castor oil-based waterborne polyurethane dispersions, Macromolecules. 46 (2013) 4606–4616.

[16] Y. Xia, R.L. Quirino, R.C. Larock, Bio-based thermosetting polymers from vegetable oils, J. Renew. Mater. 1 (2013) 3–27.

[17] H. Mutlu, M.A.R. Meier, Castor oil as a renewable resource for the chemical industry, Eur. J. Lipid Sci. Technol. 112 (2010) 10–30.

[18] K.P. Somani, S.S. Kansara, N.K. Patel, A.K. Rakshit, Castor oil based polyurethane adhesives for wood-to-wood bonding, Int. J. Adhes. Adhes. 23 (2003) 269–275.

[19] Neswati, N. Nazir, Combination of Temperature and Time in Epoxidation for Producing Epoxidized Palm Oil as Source of Bio Polyol, IOP Conf. Ser. Earth Environ. Sci. 757 (2021) 12069.

[20] J. Zhang, J.J. Tang, J.X. Zhang, Polyols prepared from ring-opening epoxidized soybean oil by a castor oil-based fatty diol, Int. J. Polym. Sci. 2015 (2015).

[21] M.A. Asare, P. Kote, S. Chaudhary, F.M. de Souza, R.K. Gupta, Sunflower Oil as a Renewable Resource for Polyurethane Foams: Effects of Flame-Retardants, Polymers (Basel). 14 (2022) 5282.

[22] Spectroscopy Study of the Crosslinking Mechanism of Cotton Cellulose, (n.d.).

[23] L.F. Marques, H.P. Santos, C.C. Correa, J.A.L.C. Resende, R.R. da Silva, S.J.L. Ribeiro, F.C. Machado, Construction of a series of rare earth metal-organic frameworks supported by thiophenedicarboxylate linker: Synthesis, characterization, crystal structures and near-infrared/visible luminescence, Inorganica Chim. Acta. 451 (2016) 41–51.

[24] A.U. Rani, N. Sundaraganesan, M. Kurt, M. Cinar, M. Karabacak, FT-IR, FT-Raman, NMR spectra and DFT calculations on 4-chloro-N-methylaniline, Spectrochim. Acta - Part A Mol. Biomol. Spectrosc. 75 (2010) 1523–1529.

[25] A.M. Awwad, N.M. Salem, A.O. Abdeen, Noval approach for synthesis sulfur (S-NPs) nanoparticles using Albizia julibrissin fruits extract, Adv. Mater. Lett. 6 (2015) 432–435.

[26] J.K. Cooper, A.M. Franco, S. Gul, C. Corrado, J.Z. Zhang, Characterization of primary amine capped CdSe, ZnSe, and ZnS quantum dots by FT-IR: Determination of surface bonding interaction and identification of selective desorption, Langmuir. 27 (2011) 8486–8493.

[27] J. Yu, S.S.C. Chuang, The structure of adsorbed species on immobilized amines in CO2 capture: An in situ IR study, Energy and Fuels. 30 (2016) 7579–7587.

[28] H. Wu, Y. Chen, W. Zhu, Y. Shangguan, Q. Zheng, Highly Adhesive and Tough Thermoplastic Polyurethanes Using a Furandicarboxamide Rigid Chain Extender with Noncovalent Interactions, ACS Appl. Polym. Mater. 5 (2023) 3515–3523.

[29] N.M. Ito, J.R. Gouveia, S.E. Vidotti, M.J.G.C. Ferreira, D.J. dos Santos, Interplay of polyurethane mechanical properties and practical adhesion of

flexible multi-layer laminates, J. Adhes. 96 (2020) 1219–1232.

[30] L.D. Antonino, I. Sumerskii, A. Potthast, T. Rosenau, M.I. Felisberti, D.J. dos Santos, Lignin-Based Polyurethanes from the Blocked Isocyanate Approach: Synthesis and Characterization, ACS Omega. 8 (2023) 27621–27633.

[31] N. Gama, A. Ferreira, A. Barros-Timmons, Cure and performance of castor oil polyurethane adhesive, Int. J. Adhes. Adhes. 95 (2019) 102413.

[32] A. Tenorio-Alfonso, M.C. Sánchez, J.M. Franco, Preparation, characterization and mechanical properties of bio-based polyurethane adhesives from isocyanate-functionalized cellulose acetate and castor oil for bonding wood, Polymers (Basel). 9 (2017) 1–14.

[33] A.M. Borrero-López, D.B. Guzmán, J.A. González-Delgado, J.F. Arteaga, C. Valencia, U. Pischel, J.M. Franco, Toward UV-Triggered Curing of Solvent-Free Polyurethane Adhesives Based on Castor Oil, ACS Sustain. Chem. Eng. 9 (2021) 11032–11040.

[34] Z. Wang, H. Kang, H. Liu, S. Zhang, C. Xia, Z. Wang, J. Li, Dual-Network Nanocross-linking Strategy to Improve Bulk Mechanical and Water-Resistant Adhesion Properties of Biobased Wood Adhesives, ACS Sustain. Chem. Eng. 8 (2020) 16430–16440.

[35] H. Liu, C. Li, X.S. Sun, Improved water resistance in undecylenic acid (UA)-modified soy protein isolate (SPI)-based adhesives, Ind. Crops Prod. 74 (2015) 577–584.

[36] Z. Xiao, Y. Li, X. Wu, G. Qi, N. Li, K. Zhang, D. Wang, X. Susan, Utilization of sorghum lignin to improve adhesion strength of soy protein adhesives on wood veneer, Ind. Crop. Prod. 50 (2013) 501–509.

[37] Y. Jang, K. Li, An All - Natural Adhesive for Bonding Wood, (2015) 431–438.

[38] M. Siahkamari, S. Emmanuel, D.B. Hodge, M. Nejad, Lignin-Glyoxal: A Fully Biobased Formaldehyde-Free Wood Adhesive for Interior Engineered Wood Products, (2022).

[39] T. Jin, H. Zeng, Y. Huang, L. Liu, D. Ji, H. Guo, S. Shi, G. Du, L. Zhang, Synthesis of Fully Biomass High-Performance Wood Adhesives from Xylitol and Maleic Anhydride, (2023).

[40] A.K. Poh, L.C. Sin, C.S. Foon, C. Cheng, Journal of Adhesion Science and Polyurethane wood adhesive from palm oil-based polyester polyol, (n.d.) 37–41.

[41] M.M. Aung, Z. Yaakob, S. Kamarudin, L.C. Abdullah, Synthesis and characterization of Jatropha (Jatropha curcas L.) oil-based polyurethane wood adhesive, Ind. Crops Prod. 60 (2014) 177–185.

[42] X. Kong, G. Liu, J.M. Curtis, Characterization of canola oil based polyurethane wood adhesives, Int. J. Adhes. Adhes. 31 (2011) 559–564.

[43] H. Chen, N. Yan, Industrial Crops & Products Application of Western red cedar (Thuja plicata) tree bark as a functional fi ller in pMDI wood adhesives, Ind. Crop. Prod. 113 (2018) 1–9.

[44] L.R. Bhagavathi, A.P. Deshpande, G.D.J. Ram, S.K. Panigrahi, Effect of cellulosic fillers addition on curing and adhesion strength of moisture-curing one-component polyurethane adhesives, Int. J. Adhes. Adhes. 108 (2021) 102871.

[45] B.B.R. Silva, R.M.C. Santana, M.M.C. Forte, A solventless castor oil-based PU adhesive for wood and foam substrates, Int. J. Adhes. Adhes. 30 (2010) 559–565.

[46] J. Peng, F. Liu, F. Feng, X. Feng, J. Cui, Enhancing Environmentally Friendly

Tannin Adhesive for Plywood through Hyperbranched Polyamide, ACS Sustain. Chem. Eng. 11 (2023) 13805–13811.

[47] B. Zhang, J. Wang, F. Zhang, L. Wu, B. Guo, Z. Gao, L. Zhang, Preparation of a High-Temperature Soybean Meal-Based Adhesive with Desired Properties via Recombination of Protein Molecules, ACS Omega. 7 (2022) 23138–23146.

[48] X. Zhao, T. Liu, R. Ou, X. Hao, Q. Fan, C. Guo, L. Sun, Z. Liu, Q. Wang, Fully Biobased Soy Protein Adhesives with Integrated High-Strength, Waterproof, Mildew-Resistant, and Flame-Retardant Properties, ACS Sustain. Chem. Eng. (2022).

[49] S. Liu, G. Du, H. Yang, H. Su, X. Ran, J. Li, L. Zhang, W. Gao, L. Yang, Developing High-Performance Cellulose-Based Wood Adhesive with a Cross-Linked Network, ACS Sustain. Chem. Eng. 9 (2021) 16849–16861.

[50] Y. Hu, Z. Kou, Y. Ma, Q. Huang, Y. Sha, M. Zhang, L. Hu, P. Jia, Y. Zhou, Hydrogen Bond-Enabled Bio-Based Random Copolymer/Carbon Nanotube Composites as Multifunctional Adhesives, ACS Sustain. Chem. Eng. 11 (2023) 13492–13501.

[51] D. Efhamisisi, M.F. Thevenon, Y. Hamzeh, A.N. Karimi, A. Pizzi, K. Pourtahmasi, Induced Tannin Adhesive by Boric Acid Addition and Its Effect on Bonding Quality and Biological Performance of Poplar Plywood, ACS Sustain. Chem. Eng. 4 (2016) 2734–2740.

[52] D.T. Allen, P. Licence, B. Subramaniam, R.M. Williams, ACS Sustainable Chemistry & Engineering Welcomes Expanded Editorial Boards with New Initiatives, ACS Sustain. Chem. Eng. 9 (2021) 1–2.

[53] Z. Duan, M. Hu, S. Jiang, G. Du, X. Zhou, T. Li, Cocuring of Epoxidized Soybean Oil-Based Wood Adhesives and the Enhanced Bonding Performance

by Plasma Treatment of Wood Surfaces, ACS Sustain. Chem. Eng. 10 (2022) 3363–3372.

[54] N. Tratnik, P.Y. Kuo, N.R. Tanguy, P. Gnanasekar, N. Yan, Biobased Epoxidized Starch Wood Adhesives: Effect of Amylopectin and Amylose Content on Adhesion Properties, ACS Sustain. Chem. Eng. 8 (2020) 17997–18005.

[55] X. Zhu, D. Wang, N. Li, X.S. Sun, Bio-Based Wood Adhesive from Camelina Protein (a Biodiesel Residue) and Depolymerized Lignin with Improved Water Resistance, ACS Omega. 2 (2017) 7996–8004.

[56] E. Cesprini, J. Jorda, M. Paolantoni, L. Valentini, P. Šket, V. Causin, D.E. Bedolla, M. Zanetti, G. Tondi, Bio-Based Tannin-Furanic-Silk Adhesives: Applications in Plywood and Chemical Cross-linking Mechanisms, ACS Appl. Polym. Mater. 5 (2023) 4468–4476.

[57] X. Zhang, C. Long, X. Zhu, X. Zhang, J. Li, J. Luo, J. Li, Q. Gao, Preparation of Strong and Thermally Conductive, Spider Silk-Inspired, Soybean Protein-Based Adhesive for Thermally Conductive Wood-Based Composites, ACS Nano. 17 (2023) 18850–18863.

[58] X. Wang, Z. Yuan, X. Pan, J. Li, Q. Tan, J. Ren, Eco-Friendly Polyurethane Reactive Hot-Melt Adhesive Derived from Poly(ϵ-caprolactone-co-lactic acid) Diols, ACS Appl. Polym. Mater. 5 (2023) 7308–7317.

[59] G. Xiao, J. Liang, Z. Wu, H. Lei, F. Gong, W. Gu, Y. Tu, D. Li, A Composite Whole-Biomass Tannin–Sucrose–Soy Protein Wood Adhesive with High Performance, Forests. 14 (2023).

[60] Z. Chang, H. Pang, A. Huang, J. Li, S. Zhang, Reinforcement of bonding strength and water resistance of soybean meal-based adhesive via construction

of an interactive network from biomass residues, Polymers (Basel). 11 (2019).

[61] R.S. Hebbar, A.M. Isloor, A.F. Ismail, Contact Angle Measurements, Elsevier B.V., 2017.